Highlights

- Ramp syncline basins were identified above thick salt in the São Paulo Plateau, Santos Basin

- They form by translation over a thick salt detachment with basal relief due to viscous drag and salt flux variations

- They record 28-32 km of SE translation during the Late Cretaceous to Paleocene

- They form by translation over basinward-dipping and landward-dipping base-salt ramps

- Stratal terminations and architecture vary along-dip and strike within these systems

1   **Geometry and Kinematics of Salt-detached Ramp Syncline Basins**

2   *Leonardo M. Pichel[1]; Frank Peel[2,3], Christopher A-L. Jackson[2,3]; Mads Huuse[1],

3

4   1 – School of Earth and Environmental Sciences, University of Manchester, Oxford
5   Road, Manchester M13 9PL, UK

6   2 – The University of Texas at Austin, Bureau of Economic Geology, Jackson
7   School of Geosciences, Austin, Texas, USA

8   3 – Basins Research Group (BRG), Department of Earth Science and Engineering,
9   Imperial College London, South Kensington Campus, SW7 2BP, United Kingdom

10

11   Corresponding author: leonardo.munizpichel@manchester.ac.uk

12   +44 (0) 7479011308

13   Frank.peel@beg.utexas.edu

14   C.jackson@imperial.ac.uk

15   Mads.huuse@manchester.ac.uk

16

17

20

21

22

23

24

25

ABSTRACT

26

27 Ramp-syncline basins (RSBs) are characterized by asymmetric depocentres
28 formed by translation above salt detachments with basal steps. Recognition of
29 these minibasins allows quantification of the magnitude and rates of overburden
30 translation above a deforming salt layer. 3D seismic data from the São Paulo
31 Plateau, Santos Basin, Brazil image a series of RSBs formed above thick salt, and
32 distributed above and/or basinward of pronounced base-salt steps. The RSBs are
33 composed of landward-dipping and gently folded sigmoidal strata, recording 28-32
34 km of SE-directed translation during the Late Cretaceous and Paleocene, at an
35 average rate of 0.8-0.9 mm/year. We present several examples of RSBs, in
36 addition to results from numerical forward models, to analyse the 3D kinematics of
37 RSBs and their interaction with base-salt structures. The RSBs form not only by
38 translation above basinward-dipping ramps, but also over landward-dipping ramps.
39 Translation over stepped ramps generates stacked RSBs. Thickness maps show
40 translation is higher at the centre of RSBs and that depocentres become
41 progressively more affected by diapirism as they evolve. This study presents the
42 first analysis of the 3D kinematics of ramp-syncline basins, and the first
43 documentation of their occurrence above thick salt in the Santos Basin, Brazil. It
44 applies realistic numerical models that treat the detachment as a volume of viscous
45 material, improving our understanding of these systems. RSBs are important to
46 understand slope and deep-basin tectono-stratigraphic architecture of supra-salt
47 units and can also guide the identification of pre-salt structures, thus contributing to
48 the exploration of salt basins.

49

50

51

52

53

1.   Introduction

Ramp-syncline basins (RSBs) are common features in extensional basins, being first recognized in the Gulf of Lyon, offshore France (e.g. Benedicto et al. 1999; Sanchis and Séranne, 2000) and the Kvamshesten Basin, onshore Norway (Osmundsen et al. 2000). They were initially described through conceptual (Gibbs, 1984) and physical models (Ellis and McClay, 1988; McClay, 1990, 1996; McClay and Scott, 1991), as forming above the hangingwall of ramp-flat extensional faults whose basal detachments dip in the direction of tectonic transport. The hanging wall is warped down above the ramp to create a relatively narrow basin. As the hangingwall block moves, the locus of subsidence (located above the footwall ramp) remains fixed in space, but its previous sediment fill is progressively moved away from it, producing a characteristic asymmetric, shingled stratal unit (Fig. 1a-b).

A second type of RSB has been identified above salt-detached systems in which the base of the moving unit is a salt layer (Fig. 1c-d) (e.g. Kwanza Basin, Angola, Peel et al. 1998; Marton et al. 1998; Jackson et al. 2001). Jackson and Hudec (2005) reviewed the processes and kinematics of RSBs on the Angolan margin using highly schematized sections and 2D seismic data. These authors described salt-detached RSBs as being formed by translation of sediments above a salt layer with a basinward-dipping ramp at its base (Fig. 1c-d). Movement over the base-salt ramp generates downwarp of the overburden, creating accommodation. Moreover, translation over two or more base-salt ramps can generate vertically stacked RSB systems (Jackson and Hudec, 2005).

Both extensional and salt-detached RSBs are characterized by an asymmetric synclinal depocentre defined by a basinward-dipping axial-trace (Fig. 1) (Jackson and Hudec, 2005). Thus, sediment layers within RSBs typically dip in the opposite direction to tectonic transport, defining "pseudo-clinoforms" (Fig. 1). The dip of the depositional axial-trace defines relative ratios of aggradation ($\square$) and translation ($\square$) rates (Jackson and Hudec, 2005). Gently-dipping axial traces indicate low $\square/\square$ whereas steeply-dipping axial traces indicate high $\square/\square$. This ratio tends to increase through time as translation rates usually decrease due to salt thinning and coeval overburden thickening (Jackson and Hudec, 2005). Although geometrically similar, extensional and salt-detached RSBs differ in terms of their stratal architecture, kinematics and the depositional settings in which they form; such aspects will be addressed in detail in this study.

The geometry and stratigraphy of RSBs can provide important information on the evolution of salt-bearing sedimentary basins. They present an excellent and potentially continuous record of the translation history of salt and overburden revealing total duration, displacement distance, speed, and direction (Hudec and Jackson, 2005). If the age of the RSB sedimentary fill is known, it is possible to identify whether the translation rate was uniform or time-variant, allowing us to accurately estimate rates of overburden translation and deformation on salt-detached gravity-driven systems (Jackson and Hudec, 2005). This can be extrapolated to more structurally complex domains, such as the updip extensional and downdip contractional provinces, where measuring total strain and unravelling the kinematic history can be significantly more problematic (Jackson et al. 2014).

4

100 Furthermore, in regions where the base-salt surface or pre-salt stratigraphy are not

101 clearly imaged, the identification of RSBs may indicate the presence, geometry and

102 location of pre-salt highs, as RSBs updip edges occur immediately above them

103 (Fig. 2). This may, in turn, assist the identification of hydrocarbon targets in pre-salt

104 highs sealed by the salt layer; which form the foundation of prolific plays in many

105 deep-water South Atlantic basins (Gomes et al. 2012; Flinch, 2014; Mohriak,

106 2015). RSBs also control slope and abyssal plain deposition and, thus, can

107 influence the distribution of hydrocarbon reservoirs in supra-salt intervals. Salt-

108 detached gravity-driven translation causes a seaward-shift of supra-salt strata,

109 which can result in juxtaposition of supra-salt sandier intervals initially deposited on

110 the shelf and upper-slope, above mature pre-salt source rocks on the lower-slope

111 and deep-basin (Fig. 2). If a salt weld is formed below the RSB, these supra-salt

112 reservoirs can be charged by hydrocarbon migration from the pre salt section

113 (Rowan 2004; Jackson et al. 2014). Wherever RSBs are present, one cannot fully

114 understand supra-salt stratigraphic architecture without understanding the

115 kinematics of RSBs.

116 Despite their notable value for both academia and industry, there has been little

117 further research on RSBs since Jackson and Hudec (2005). For example, there

118 has been no investigation of the 3D kinematics and stratigraphic architecture of

119 natural RSBs, or physical or numerical modelling to constrain the few previous

120 observations. Moreover, very few studies have documented RSBs outside their

121 type-area in the Kwanza Basin: Rowan (2014) in the Red Sea and Dooley et al.

122 (2016) in the Campos Basin, Brazil. Nevertheless, we contend RSBs have been

123 shown in previous works without being explicitly recognized and/or studied in detail

124 (Alves et al., 2016; Jackson and Hudec, 2017).

125 Here we present the first documentation of RSBs in the Santos Basin, Brazil

126 providing a detailed analysis of their 3D geometry, stratigraphic architecture, and

127 kinematics. We present seismic sections and thickness maps of the RSBs, then

128 compare their geometries with numerical forward models simulating cover

129 translation above a salt detachment with variable topography and thickness. These

130 models provide a more comprehensive and realistic evolution of RSBs, as they

131 treat the detachment as a volume of deforming viscous material (Fig. 1c-d), rather

132 than a discrete, undeformable surface (Jackson and Hudec, 2005). This allows us

133 to evaluate the role of diapirism and salt flux variations on RSB evolution.

134 Ultimately, this work aims to improve our current understanding of RSBs and to

135 provide a guide for their identification and analysis in other settings and basins.

136 **2. Tectono-Stratigraphic Framework of the São Paulo Plateau**

137 The São Paulo Plateau (SPP), Santos Basin (Fig. 3) is an area of thick, layered

138 Aptian salt (Gamboa et al., 2009; Davison et al. 2012; Fiduk and Rowan, 2012;

139 Jackson et al. 2014; 2015) and a complex, polygonal pattern of salt diapirs (Guerra

140 and Underhill, 2012; Jackson et al. 2015). The area is a prolific hydrocarbon

141 province, with discoveries in both pre- and post-salt reservoirs, including some of

142 the largest oil discoveries in the last decades (e.g. Tupi and Iracema fields) with

143 reserves over 5 bbl in pre-salt structural highs (Mohriak et al. 2012).

The basin is characterized by a series of NE-oriented graben and half-graben formed during late Barremian-early Aptian rifting. These basins are filled by non-marine clastic strata and are overlain by shallow-marine carbonates (Meisling et al. 2001; Modica and Brush, 2004; Karner and Gambôa, 2007; Mohriak et al. 2008, 2009; Contreras et al. 2010). During the late Aptian, most rift-related faults became inactive and a 1 - 3 km thick post-rift salt succession was deposited (Davison et al. 2012). During the early Albian, the Santos Basin experienced fully marine conditions due to thermally-induced subsidence and eustatic rise. This resulted in widespread deposition of a carbonate-dominated succession expressed as a fine-grained, marl-dominated succession (Modica and Brush, 2004). During the latest Albian, thermal and isostatic subsidence tilted the basin south-eastward, inducing salt-detached gravity gliding and the development of thin-skinned, predominantly seaward-dipping normal faults that dismembered the Albian carbonate platform updip of the study area (Demercian et al. 1993; Cobbold et al. 1995; Mohriak et al. 1995; Guerra and Underhill, 2012; Quirk et al. 2012).

During the Cenomanian-Turonian, drowning of the carbonate platform, in response to a rapid eustatic rise and thermal subsidence, resulted in extensive deposition of shales and marls (Modica and Brush, 2004). Throughout the Late Cretaceous to Paleocene, and despite a continued eustatic sea-level rise, sedimentation was dominated by siliciclastic progradation due to uplift of the Serra do Mar mountain range, with extensive turbidite deposition during the late Campanian (Modica and Brush, 2004). By end Paleocene, sea-level fall resulted in the development of a major regional unconformity, leading to erosion and basinward redistribution of

shelf and slope sediments. Inflated salt on the SPP acted as a topographic barrier to basinward transportation of coarse clastics from the end of the Paleocene onward (Modica and Brush, 2004), resulting in widespread mud deposition in more distal locations.

The SPP is situated at the present-day toe-of-slope, immediately downdip of the Albian extensional domain and the Albian Gap (Fig. 3) (Quirk et al. 2012; Jackson et al. 2015). Some authors suggest regional shortening of the supra-salt cover on the SPP continued throughout the entire late Cretaceous (Quirk et al 2012; Fiduk and Rowan 2012; Guerra and Underhill, 2012; Alves et al. 2017). Others argue Late Cretaceous deformation was dominated by salt inflation and density-driven processes, with only local contraction and extension (Ge et al. 1997; Gemmer et al. 2004; Jackson et al 2015; Dooley et al 2015). However, the aspects and magnitude of salt-related basinward translation of the SPP and its effects on minibasin development have not yet been studied.

3.   Methods

3.1.   Seismic Interpretation

This study uses a zero-phase processed, time-migrated, 3D seismic reflection dataset covering 20,122 km^2 of the SPP, Santos Basin, Brazil. Inline (west-east) and crossline (north-south) spacing is 18.75 and 25 m, respectively. The vertical sampling interval is 4 ms two-way time travel (ms TWT), and total record length analysed is 5500 ms TWT. The survey display follows the Society of Economic Geologists normal polarity, where a downward increase in acoustic impedance is

189 represented by a positive reflection event (white on greyscale seismic sections)

190 and a decrease in acoustic impedance by a negative event (black on greyscale

191 seismic section) (Brown, 2011).

192 The average dominant frequency in the Aptian salt is c. 36 Hz and the interval

193 velocity is c. 4400 m/s, yielding a vertical resolution of c. 29 m (Rodriguez et al.,

194 2017). The relatively lower velocity of the salt is due to the intra-salt lithological

195 heterogeneity and, more specifically, the presence of acoustically slower potash

196 intervals (Jackson et al., 2015). Overburden strata have a dominant frequency that

197 varies with depth from c. 40-31 Hz and a slower average interval velocity (c. 1900-

198 2015 m/s), which together result in higher vertical resolution (c. 12-17 m) that

199 decreases with depth (Jackson et al., 2015; Rodriguez et al., 2017). Horizontal

200 resolution is twice the seismic line spacing (i.e., 37.5 m in the E–W direction and

201 50 m in the N–S direction) (Jackson et al 2015).

202 In order to constrain the geometry, and to understand the 3D kinematics and

203 tectonostratigraphic evolution of RSBs, 3D seismic mapping of key surfaces within

204 the RSBs were produced to generate thickness maps of key stratigraphic intervals.

205 We did not use primary well data, with the identification of key seismic stratigraphic

206 surfaces, such as the top and base salt (Figs. 4 and 5a), top Albian, the intra-

207 Paleocene unconformity and top Paleocene, being based on previous publications

208 (Fiduk and Rowan, 2012; Guerra and Underhill, 2012; Jackson et al. 2015). Intra-

209 RSB horizons were chosen based on their reflectivity and continuity.

210 **3.2. Base-salt map**

211 It was vital to have a detailed base-salt map in order to match the observed RSBs

212 to the base-salt topography responsible for their formation. Although the top and

213 base-salt surfaces were readily identified and interpreted in TWT; the presence of

214 a thick, deformed evaporite layer, whose velocity is generally higher than the

215 overlying sediments, introduces distortion of the base-salt and pre-salt section

216 such that the real structure is obscured by velocity pull-ups. Although, in places,

217 syn-rift structures (i.e. normal faults and wedge-shaped intervals) help constrain

218 the location of pre-salt structures (Figs. 6-8), in other areas they could not be

219 readily identified in our TWT base-salt map.

220 Publically available depth-maps (e.g. Alves et al. 2016, fig. 5b) do not cover the

221 entire study-area nor do we have access to a reliable, high-resolution velocity grid

222 to create maps by conventional depth-conversion. Instead, we developed a reliable

223 base-salt structure map (Fig. 5a) by stretching the thickness of salt by a factor of

224 1.61 and shifting the base salt accordingly. This is equivalent to a static correction,

225 in which the salt velocity is reduced by 39%. The resulting map is in TWT (Fig. 5a),

226 not depth, representing where the base-salt would be if salt was replaced by an

227 equivalent thickness of sediment. The appropriate factor was obtained iteratively

228 by finding the value that best removed the most evident velocity pull-ups. Finally, a

229 gentle spatial smoothing factor was applied to remove the effect of non-vertical ray

230 paths, which created local high-frequency spikes under the steeply-dipping flanks

231 of salt bodies (Jones and Davison, 2014). The best indicator that our approach was

232 effective is that the resulting map (Figure 5a); (i) shows no discernible imprint of

233 the overlying salt structure; (ii) compares favourably to the depth-map presented by

234 Alves et al. (2016) (Fig. 5b); and (iii) to a regional, 2D, depth-migrated seismic

235 profile (Fig. 6). Four major base-salt highs are identifiable on the map; each

236 bounded updip and downdip by base salt ramps (Fig. 5). This result compares well

237 with the interpretations shown by Davison et al. (2012) and Alves et al. (2017),

238 both of whom use depth data.

239 **4.   Observations (Ramp-Syncline Basins)**

240 Both simple (section 4.1.) and stacked RSBs (section 4.2) were identified above

241 thick salt (1.5-2 km) on the SPP, distributed above and basinward of the main

242 base-salt steps (Figs. 4-5). These basins trend NNE to NE (Figs. 4-5), and are

243 composed of 9-20 km wide by 15-35 km long continuous panels of landward-

244 dipping and thickening strata that become younger landward (Figs. 6-12). The

245 RSBs contain stratigraphic successions up to 600 ms (~700 m) thick (Fig. 8); with

246 average thickness of 400 ms (400-450 m, figs. 7 and 9-11); this corresponds to 25-

247 35% of total post-salt succession (Fig. 12a).

248 The base-salt steps associated with the RSBs trend mainly NNE-NE, parallel to the

249 RSBs, although the northernmost high trends NNW and, thus, slightly oblique (Fig.

250 5a-b). These steps have approximately 0.5-2 km of structural relief, dipping

251 predominantly landward to the west and basinward to east within the study-area,

252 being associated with a large pre-salt structure known as the Outer High (Fig. 6)

253 (Gomez et al., 2012). In this study, we present the five least deformed, largest, and

254 thus best imaged examples of RSBs in order to analyse their 3D geometries,

255 kinematics, tectono-stratigraphic evolution, and interaction with base-salt

256 structures.

4.1. Simple Ramp-Syncline Basins

258 Simple RSBs are characterized by asymmetric sigmoidal growth strata dipping and

259 expanding landwards towards a diachronous basal boundary (Figs. 7-9). The

260 RSBs are capped by a diachronous top unconformity and terminate landward

261 above a base-salt ramp that may dip basinward (Fig. 7) or landward (Figs. 8-9).

262 Their depositional axial-trace dips predominantly basinward, becoming broadly

263 steeper landward within the uppermost strata and with minor switches in their dip-

264 direction due to simultaneous diapirism, folding, and rotation (Figs. 7-9 and 12b). In

265 the majority (85%) of RSBs, lowermost strata onlap against the top of the broadly

266 isopachous, 300-400 m thick, Albian succession (Figs. 7 and 9-11). In the other

267 RSBs, the first onlaps are against younger, Late Cretaceous strata (Fig. 8, and

268 landward panels of figs. 9 and 11).

4.2. Stacked Ramp-Syncline Basins

270 In the north-central and northeast of the study-area, RSBs are characterized by

271 stacked onlap surfaces and ramp-syncline strata (Figs. 10 and 11), being more

272 complex than the ones further south. They are located above pairs of basinward-

273 dipping ramps (Fig. 10), and above a NNW-trending pre-salt horst block defining

274 landward and basinward-dipping base-salt ramps (Figs. 5 and 11). The

275 stratigraphic architecture of stacked RSBs is similar to simple RSBs described

276 previously (Figs. 7-9), with landward-dipping sigmoidal growth strata defined by a

277 predominantly basinward-dipping axial-trace (Figs. 10, 11 and 12c). The lower

278 RSB terminates updip above the landwardmost base-salt ramp, whereas the upper

279 RSB terminates over the basinwardmost base-salt ramp (Figs. 10, 11 and 12c).

280 The unconformity bounding the top of the lower, landward RSB acts as the basal

281 onlap surface for the upper RSB along most of the stacked section, being

282 commonly separated by a thin drape interval updip (Figs. 10, 11 and 12c).

283 **5. Interpretation**

284 Simple RSBs are interpreted to form by salt-related translation above a single

285 base-salt ramp, whereas stacked RSBs form by simultaneous translation above

286 two or more base-salt ramps, as in examples from their type-area in the Kwanza

287 Basin, Angola (Jackson and Hudec, 2005). The lower, landward RSB forms by

288 translation above the landward ramp, whereas the upper, basinward RSB forms by

289 translation above the basinward ramp. If the distance between base-salt ramps is

290 smaller than the amount of translation, the updip portion of the basinward RSB

291 overlaps the downdip portion of the landward RSB, generating stacked RSBs

292 (Figs. 10-11). Thus, the distance between steps is inversely proportional to the

293 width of the stacked RSB section. Deposition occurs simultaneously within both

294 stacked RSBs, so the first and last deposited strata, and equivalent onlap points in

295 each RSB have the same age and, accordingly, the amount of translation recorded

296 by each RSB is the same (Jackson and Hudec, 2005). Along-strike correlation

297 around salt walls indicate that, in some cases (Figs. 8-11), RSB panels now

298 separated by salt walls can form by translation above the same base-salt ramp

299 (Fig. 12a-b), being subsequently segmented by synchronous-to-subsequent

300 diapirism. In these cases, the landward panels are composed of younger strata

301 onlapping a thicker and younger pre-translation section relative to their basinward

302 and older panels (Figs. 8-11) (c.f. Jackson and Hudec, 2005).

303 Translation above a thick salt detachment is driven by viscous drag within the salt

304 (Rowan et al., 2004; Peel 2014), which simultaneously produces localized rotation,

305 cover deformation, and diapirism (Dooley et al., 2016). These processes are

306 represented in our study-area by faulting at the flanks and/or crests of diapirs, and

307 folding and rotation of RSB strata, generating additional complexities and acting as

308 secondary controls on the evolution of RSBs. Additionally, as RSBs form above a

309 thick salt interval, density-driven processes such as salt expulsion and inflation

310 occur in tandem with translation and RSB development (Jackson and Hudec,

311 2005). We see this where RSBs have a more symmetric geometry, usually in their

312 uppermost sections (Figs. 7-11), and where salt has drastically thinned beneath

313 them (SE edge of RSB 3, Fig. 9).

314 **5.1. Stratal Variation within RSBs**

315 In both simple and stacked RSBs, stratal termination can vary along dip and strike

316 (Figs. 7-11). Thus, in this section we present a summary of the stratigraphic

317 architecture and terminations for both simple and stacked systems (Fig. 12). Lower

318 boundaries are generally characterized by a well-defined, diachronous onlap

319 surface that becomes younger landward (Figs. 9-11). Apparent downlaps are

320 typical of the lowermost RSB fill, which has been progressively rotated during

321 translation (Figs. 7-11) whereas original onlap relationships are most easily

discerned for the younger and, thus, less rotated packages preserved in landward

positions (Figs. 7-11). In places, the basal boundary is defined by a transition from

a thicker, landward-dipping section to a drape interval that has the regional dip

(Figs. 9-11 and 12b-c). We thus interpret the apparent downlaps as originally

forming as onlaps against paleo-bathymetric highs and/or diapirs above base-salt

ramps. These terminations dominate where strata are older and consequently have

been translated further and rotated more.

Like the lower boundaries, the upper RSB boundaries also become younger

landward, being defined in places by erosional truncation, most commonly in the

downdip part of the system where strata are usually steeper (orange to blue

horizons, fig. 8c-d). Elsewhere, the upper boundary is defined by toplaps (light-blue

horizon, fig. 8c-d) or, most commonly in the updip portions of the system, by an

abrupt transition from a thin, draping section of regional dip, to a thicker, more

steeply-dipping section (light-orange horizon, fig. 8). Steep stratal dips and

erosional truncation are possibly caused by a combination of: i) uplift due to salt

drag (see model in fig. 1c-d) and/or salt inflation at the edge of the RSB; and ii) a

higher degree of translation and rotation of older RSB strata.

A landward shift from abrupt to subtle transitional limits along the upper and lower

boundaries of the RSBs (Fig. 12b-c) is explained by an increase in the

aggradation/translation ratio ($\square/\square$). This is evidenced by landward steepening of

the depositional axial-trace in areas where the RSBs are less folded (Fig. 7-11).

Additionally, as the RSBs evolve and $\square/\square$ increases, the overburden thickens such

that loading and salt expulsion become progressively more important control on

345 their evolution. As in simple RSBs, the boundaries of each stacked RSB can be

346 defined by a transition from steeper, thickened section within the RSB, to thin,

347 draping strata away from it (Figs. 10 and 11b). This explains the development of

348 thin drape intervals separating the lower RSB top unconformity from the upper RSB

349 onlap surface (Figs. 10 and 11), typically in their uppermost sections (Fig. 12c).

350 **5.2. Translation history and depocentre migration**

351 To analyse RSB kinematics, we present true-stratigraphic thickness maps from the

352 largest example found within the area (RSB 5, figs. 11 and 13), which is the best

353 representative of all others RSBs mapped. The isopachs are located basinward of

354 or above base-salt ramps with the main depocentres having similar trends and

355 shapes (Fig. 13). They present consistent amounts (1.8-3.1 km) and directions of

356 offset (120 $\pm$ 15°), through time, towards the SE-ESE, which is parallel to the

357 regional gravity-driven tectonic transport direction (Quirk et al 2012; Jackson et al

358 2014), roughly perpendicular to the trend of the main base-salt steps. The

359 constancy of these values indicates these depocentres likely formed in response to

360 a single, relatively steady SE-ESE-oriented process (i.e. basinward translation over

361 base-salt relief).

362 By summing the offsets between the thickest points on each isochron map in fig.

363 13, a total translation of 26.9 km was obtained for RSB 5. This, however,

364 represents a minimum distance as we were not able to include isopachs of the first

365 and last onlapping intervals, due to intense faulting and folding at both their eastern

366 and western edges (Figs. 11 and 13). Nevertheless, it was possible to obtain

16

367 confident translation estimates for each RSB by measuring the distance of their

368 first onlap points to the top of their corresponding ramps, (c.f. Jackson and Hudec,

369 2005). RSB 5 records the larger amount of translation of all RSBs on the SPP,

370 estimated at 32 (± 2) km (Fig. 11 and 13). In many other examples, we were only

371 able to determine a minimum translation because they are located at the eastern

372 edge of the data, such as in RSB 1 (9.5 km of translation), RSB 2 (18 km) and RSB

373 4 (16 km); or are eroded or heavily deformed by diapirism. Nonetheless, less-

374 deformed and less–eroded examples situated more centrally in our dataset allowed

375 more precise estimates of cover translation in the area, which varied from 28 km in

376 the south (RSB 3, fig. 8) to 32 km to the north (RSB 5, fig. 11). Stacked RSBs were

377 important to guarantee a higher degree of certainty in areas of complex salt

378 deformation or erosion, as they record the same amount of translation (Jackson

379 and Hudec, 2005) and, thus, can be used as a cross-check. As seen in RSB 5,

380 both landward and basinward RSBs document 32 km of translation (Fig. 11).

381 Thickness maps also demonstrate the discrepancy between the vertical and true

382 (i.e. stratigraphic) thickness of strata preserved in the RSBs. RSB 4, for example,

383 has a vertical thickness of c. 500 ms (Fig 10), but, by adding the true thickness of

384 each of its mapped intervals, a total of 2130 ms (c. 2400 m) (> 4 times its vertical

385 thickness) is obtained. This contrast occurs because, as RSB strata translate, they

386 rotate and move away tens of kilometres from where they were originally

387 deposited; while new sediments accumulate at the fixed depocentre. As RSBs are

388 capped by Top-Cretaceous or Intra-Paleocene erosional unconformities (Figs. 6-

389 11), stratigraphic thicknesses preserved within them likely represent a minimum.

390   Using age constraints provided by Modica and Brush (2004); Guerra and Underhill,

391   (2012) and Jackson et al. (2015), and the observation that oldest RSB strata onlap

392   the Albian section, we suggest translation commenced at the end of the Albian.

393   Furthermore, we estimate the end of translation to vary from end Cretaceous (Fig.

394   7) to middle Paleocene (Fig. 8-11). Although there is a degree of uncertainty

395   regarding these age estimates, we can obtain an approximate average translation

396   rate of 0.7–0.8 mm/yr (0.7-0.8 km/Myr.).

397   **6. RSB Modelling and Kinematics**

398   Our seismic based observations from the Santos Basin were compared with

399   forward models reproducing what we inferred as the main process generating

400   RSBs, i.e. cover translation above a thick salt detachment. Numerical models have

401   been used extensively in salt tectonics studies, providing important insights into the

402   sequential evolution of salt structures and the mechanics of salt flow (Gemmer et

403   al., 2004, Albertz and Ings, 2010; Gradmann and Beaumount, 2015; Weijermars et

404   al., 2015; Pichel et al., 2017). Our simulations allowed us to evaluate the

405   kinematics and processes controlling the development of RSBs, and to confirm that

406   the observed geometries could be interpreted in the context of the interpreted

407   base-salt topography. In our models, translation of the cover is accommodated by

408   layer-parallel shearing of the whole thickness of the salt, i.e. Couette flow

409   (Weijermars, 1993; Cotton and Koyi, 2000; Rowan et al. 2004; Weijermars et al.,

410   2015), as opposed to movement on a fault (McClay, 1990; 1996) or a discrete

411   detachment (Jackson and Hudec, 2005).

412 Modelling was performed using SaltDragon©, a novel application created in

413 Microsoft Excel©. This application provides a simple but effective 2D model of the

414 stratal geometries produced in RSBs by simulating viscous salt drag and

415 overburden translation above a salt detachment with variable thickness and basal

416 topography. The geometry of the decollement and the rate of sediment

417 accumulation can be adjusted in order to replicate the general form of the natural

418 RSBs observed in seismic data, and to investigate the possible controls on RSB

419 geometry. The application is non-dimensional (i.e. scale-independent), so the

420 computations relate to grid cells, and are valid regardless of the dimension of the

421 grid or vertical scaling factor.

422 The overburden is offset horizontally, one grid cell per time increment, over the

423 viscous decollement, with an initially uniform top and a base of user-defined

424 irregularity. The pre-salt interval remains fixed and rigid. The post-salt pre-

425 translation interval is tabular, and syn-kinematic sedimentation is added

426 continuously and at a constant rate through time. After each increment, the

427 overburden is deformed by vertical shear to maintain contact with the top of the

428 salt. The height of the new sediment depositional surface at each point in time is

429 user-defined. The calculated accommodation (space between the new depositional

430 surface and the top surface of the deformed overburden) determines the thickness

431 of new sediment deposited in each increment. There is no compaction or erosion in

432 this model, and the depositional surface is presumed to be planar and uniformly

433 dipping, which is likely applicable to the deep-water settings considered in our

434   natural example. The process is repeated sequentially, creating a complete

435   realisation of the evolution of the system.

436   The shear strain associated with the layer-parallel shearing within the salt is

437   assumed to be uniform throughout each vertical column (Fig. 14). Thus, where salt

438   is thinner, the total flux of dragged salt is lower than where the salt is thicker and

439   *vice versa* (Fig. 14). As the original salt thickness changes across base-salt

440   topography, the overall salt flux also changes (Dooley et al. 2016). As a result,

441   parts of the section may experience net loss or gain of salt, resulting in salt

442   thickness variations, and subsidence or uplift of the overlying sediments (Fig. 14).

443   This controls the deposition and stratigraphic architecture of syn-kinematic strata,

444   and the development of RSBs.

445   Because the models begin with a planar top-salt surface, the generation of

446   subsidence and uplift in the initial stages is entirely due to the effect of salt drag

447   and laterally varying salt flux (Figs. 14a-b). However, as the model evolves,

448   significant topography is created on the top salt surface and a second factor,

449   vertical movement, comes into play. The cover moves with a downward component

450   where the top-salt dips in the direction of tectonic transport, and an upward

451   component where the top of salt dips in the opposite direction (Figs. 14c). This

452   produces local subsidence and uplift, in addition to those created by local thinning

453   or thickening of salt. An important consequence of this is that regions of local uplift

454   can develop on the downdip side of RSBs, even where the cover is moving over a

455   basinward-dipping ramp (Fig. 14c-d). This is recognized in the Santos Basin by

456   development of prominent erosional unconformities on the downdip sides of RSBs

457   1, 4 and 5 (Figs. 7, 10 and 11).As top-salt relief develops, the amount and extent of

458   uplift should progressively increase (Figure 14c-d). In nature, a combination of

459   Couette and Pouiseuille salt-flow would intensify the uplift as salt would be laterally

460   expelled from beneath the RSB, resulting in inflation and diapirism at its edges.

461   Whilst the models appear to broadly reproduce the main geometries observed in

462   the Santos Basin, they do not reproduce the entire kinematics of the system. In

463   particular, these models do not replicate diapirism and Pouiseuille-flow driven by

464   differential loading. Also, our models assume: 1) the overburden neither stretches

465   nor shortens laterally as it moves, 2) the overburden has very little resistance to

466   vertical shear, so there is no salt return Poiseuille-flow component, as would be the

467   case with a more rigid roof; and 3) the pre-translation interval is perfectly tabular

468   and isopachous. Nevertheless, separating the contribution of one factor alone

469   (entrainment of the viscous decollement layer by drag, modelled as Couette flow)

470   allows us to explore the influence of this important component of salt tectonics.

471   Furthermore, the fact that this approach produces results that are remarkably

472   similar to RSBs observed in both the Santos and Kwanza basins, suggests it is a

473   valid first-order approximation of the dynamics of these systems.

474   We present four models testing the effects of different base-salt topography and

475   variable salt thickness on overburden translation, deformation and stratigraphic

476   architecture. Model 1 simulates translation above a basinward-dipping ramp, and

477   model 2 reproduces translation above a pair of basinward-dipping ramps. In Model

478   3, we evaluate translation over a landward-dipping ramp and, in Model 4,

479   translation over a base-salt horst defined by landward- and basinward-dipping

480   base-salt ramps.

6.1. Model 1 (single basinward-dipping ramp)

482   In Model 1, salt and overburden translate over a basinward-dipping ramp. As salt is

483   thinner updip of the step (Figs. 14a and 15), less salt is dragged into the step than

484   out of it (Dooley et al. 2016). This salt deficit results in local salt thinning and cover

485   subsidence (Fig. 14a and 15a-b), and the generation of an asymmetric depocentre

486   above the ramp. As translation continues, previously deposited strata are moved

487   out of the ramp while new sediments are deposited immediately above it. This

488   results in the development of a RSB, characterized by an asymmetric growth

489   interval that dips and expands landwards towards a diachronous basal boundary.

490   The top of the RSB is being truncated by a diachronous unconformity (Fig. 15c-d),

491   similar to examples from the SPP (Fig. 7-9).

492   The axial-trace and bounding surfaces are sub-parallel (Fig. 15d). Initially, they dip

493   gently in the direction of tectonic transport, i.e. basinward (Fig. 15b) but, as

494   translation progresses, salt drag and uplift rotate them, flipping their dip direction,

495   i.e. landward, at the downdip edge of the system (Fig. 15c and d). Because in the

496   model translation and sedimentation rate are constant, this change in geometry

497   happens entirely in response to shear drag, and the consequent upward translation

498   and rotation of syn-kinematic strata. In reality, folding and rotation of RSBs internal

499   intervals and surfaces can be even more pronounced due to a combination of: i)

500 variations in □/□, ii) salt expulsion and diapirism, and ii) overburden extension and

501 contraction.

502 Basal surfaces of salt-detached RSBs are usually diachronous and shingled (i.e.

503 not a discrete surface as in extensional RSBs (McClay, 1990; 1996) as sediments

504 may also be deposited upslope of the RSB in the form of a thin drape fringing the

505 main depocentre (Fig. 15c and d). In our seismic examples, thin drape horizons

506 usually occur at the updip portions of the systems, being usually 1-2 seismic

507 reflections thick (Figs. 8-11), equivalent to only a few tens of meters.

508 Model 1 is also run with a higher □/□ to illustrate how varying the relative rates of

509 aggradation and translation produces different RSB stratal architectures (Fig. 16).

510 Translation rate (□) is kept constant while aggradation rate (□) is increased 3-fold

511 (Fig. 16a-b). When □/□ is low, the RSB is more asymmetric, and its boundaries

512 are defined by abrupt strata terminations and diachronous unconformities (Fig.

513 16a). The basal boundary is an onlap surface whereas the top boundary is defined

514 by offlap/toplap geometries. Conversely, when □/□ is high, the RSB is less

515 asymmetric, the synclinal axial-trace is steeper, and diachronous boundaries are

516 characterized by a transition from a thicker, steeper section within the RSB to

517 thinner intervals at regional dip outside it (Fig. 16b). If □ is higher than □, local

518 uplift on the downdip side of the RSB is not enough to generate sea-floor exposure

519 and erosion (Fig. 16b), which in a deep-water setting such as on the SPP, could be

520 driven by sea-bottom currents. Although not shown here, variations of

521 sedimentation rate during the development of RSBs can also produce intra-RSB

522 unconformities and offlap terminations.

6.2. Model 2 (two basinward-dipping ramps)

Model 2 simulates cover translation above a thick salt layer with two closely-spaced, base-salt basinward-dipping ramps (Fig. 17). Basin geometry and evolution above each base-salt ramp is similar to Model 1, such that a landward RSB forms above the landward ramp while a basinward RSB develops above the basinward ramp (Fig. 17b-c). As translation continues, these basins are vertically juxtaposed, forming stacked RSBs (Fig. 17c-d) (c.f. our seismic examples in figs. 10-11). Deposition occurs simultaneously within both RSBs (Fig. 17b-d), which means the first and last deposited strata, and respective onlap points in each of the stacked RSBs, have the same age and, accordingly, record the same amount of translation (Fig. 17) (Jackson and Hudec, 2005).

The basinwardmost interval of each RSB corresponds to older strata that have translated further and are, therefore, more rotated and uplifted by shear drag than younger intervals (Fig. 17). If the aggradation rate is lower than the rate of salt movement, salt drag results in exposure of the basinward side of each RSB (Fig. 17d), leading to localized erosion, (c.f. our natural examples, i.e. landward and basinward RSBs in fig. 11 and landward RSB in fig. 10). The width of the exposed area is smaller in the landward RSB, presumably because it is progressively and partially buried by the basinward RSB strata, onlaping onto the landward RSB top unconformity (Fig. 17d).

Our model shows that the lower, landward RSB top unconformity acts as the basal onlap surface of the upper, basinward RSB (dashed black line in fig 17d) (c.f. figs.

545 10 and 11). When the sedimentation rate is lower than the translation rate, the

546 stacked RSBs top unconformities merge landward, and their basal onlap surface

547 merge basinward (Fig. 17). Although there is a level of uncertainty due to the

548 presence of folds and diapirs in the study area, this pattern is seen in portions of

549 RSB 5 (Fig. 11a-b), where the RSB interval is thinner. When sedimentation rate is

550 relatively high, a thin drape interval can separate these boundaries (Fig. 10).

551 As seen in Model 2, each RSB terminates landward above the top of its respective

552 ramp (Fig. 17d). This is seen in many of our seismic examples (LW ramp and

553 middle ramp RSBs in Fig. 11), although, in some areas, diapirism and overburden

554 deformation can laterally offset their landward edges from the top of their

555 respective ramps by up to 1-2 km (Fig. 10). These complexities, however, lead to

556 only a minor amount of uncertainty when compared to the total translation of these

557 systems (see section 5.2.) and are, therefore, not enough to invalidate our

558 translation estimates.

559 **6.3. Model 3 (Landward-dipping Ramp)**

560 Model 3 simulates cover translation above a thick salt detachment with a landward-

561 dipping basal step, generating similar syn-kinematic stratal geometries to Model 1.

562 However, in this case, the RSB forms immediately basinward of the ramp, above a

563 base-salt flat (Fig. 18), instead of above the ramp as in Models 1-2 (Fig. 14-17) (c.f.

564 RSBs 2-3 in figs. 7 and 8). As salt moves from an area of thick to thin salt across

565 the ramp, more salt is dragged into the ramp than out it (Figs, 14b and 18a-b)

566 (Dooley et al. 2016). This salt surplus results in salt thickening and cover uplift

567 above the ramp, and generation of accommodation around the salt anticline

568 formed over the ramp. As translation continues, more salt is fed into the anticline,

569 causing it to widen basinward without leaving its original position. Thus, whilst its

570 landward flank remains static, the basinward flank translates and acts as a

571 basinward-dipping ramp forming an asymmetric depocentre above it. Syn-

572 kinematic strata onlap and thicken towards this flank, while being progressively

573 rotated and translated basinward (Fig. 18b-c).

574 The geometry and evolution of the asymmetric growth interval are notably similar

575 to RSBs formed above basinward-dipping ramps (compare figs. 15 and 18) and to

576 natural examples of RSBs formed above landward-dipping steps (Figs. 7 and 8).

577 These RSBs are composed of shingled sigmoidal strata that dip and expand

578 landward, being located basinward of a landward-dipping base-salt ramp and

579 above a base-salt flat (Figs. 7 and 8). They are bound on their landward edge by a

580 wide diapir (Fig. 7) or salt anticline (Fig. 8), which are situated directly above the

581 top of the ramp (c.f. fig. 18).

582 In Model 3, the salt anticline remains static but, in reality, it may translate downdip

583 after reaching enough thickness and, thus accelerating (Dooley et al., 2016), with a

584 younger salt structure forming updip, above the ramp. After leaving the ramp, the

585 salt anticline may be reactivated by extension, as shown in physical models

586 (Dooley et al. 2016) and seen in seismic examples from the SPP (mid-RSB diapirs

587 in Fig. 8). As the anticline grows and its roof is uplifted above regional, outer-arc

588 extension and erosion (not modelled) can thin the roof and allow diapiric

589 piercement as seen in RSB 2 and 3 (Figs. 7 and 8).

590 The apparent offset of synkinematic strata across the diachronous onlap surface

591 above the anticline could be erroneously interpreted as a basinward-dipping listric

592 fault (Fig. 18c-d). However, natural examples and models show that this geometry

593 is entirely formed in response to differential uplift and sedimentation during cover

594 translation. As salt thickens above the ramp, sediments are deposited around the

595 anticline while the area above it is uplifted and remains sediment starved (Fig. 18).

596 This pattern in is observed in natural examples from the SPP, where RSB strata

597 are separated from equivalent-age non-RSB strata landward by salt walls and/or

598 anticlines (Fig. 8).

599 **6.4. Model 4 (Base-Salt High)**

600 Model 4 illustrates the development of stacked RSBs formed by translation over a

601 horst-like high, defined by a landward-dipping ramp updip and a basinward-dipping

602 ramp downdip (Fig. 19, c.f. RSB 5, fig. 11). Translation across the landward step

603 results in salt thickening above the step and development of a RSB basinward of it,

604 whereas translation over the basinward step results in salt thinning and

605 subsidence, with generation of another RSB above it. As translation progresses,

606 these minibasins overlap and stacked RSBs are formed.

607 Whereas the basinward RSB is very similar to previous models of basinward-

608 dipping ramps (Figs. 15 and 19), the geometry of the landward RSB is different to

609 that produced in Model 1. More specifically, because the landward RSB moves

610 over the second, basinward-dipping step, it subsides and rotates further, thus,

611 dipping more steeply basinward (Fig. 19). This is seen in RSB 5 where the lower,

612 landward RSB is steeper above the basinward-dipping ramp, being limited by a 5

613 km wide salt wall (Fig. 11).

614 **7. Discussion**

615 **7.1. Dynamics of RSBs in the Santos Basin**

616 We mapped a series of asymmetric minibasins characterized by landward-dipping

617 and expanding sigmoidal growth strata distributed parallel, above and/or downdip

618 of the main base-salt steps in the study-area, (Figs. 4-11). Similar minibasin

619 architectures were previously recognized over relatively thinner salt in the Kwanza

620 Basin, as formed by translation above basinward-dipping base-salt ramps (Fig. 20)

621 (Peel et al., 1998; Marton et al., 1998; Jackson and Hudec, 2005). We used

622 numerical models to simulate this process (i.e. translation and salt flux variations

623 driven by viscous drag over base-salt ramps) and to test the supra-salt

624 stratigraphic response. Modelling results produced remarkably similar minibasin

625 geometries and relationship with base-salt topography to natural examples from

626 the study-area (Figs. 6-11 and 15-19) and Kwanza Basin (Fig. 20). Models and

627 seismic data, thus, provide evidence that these minibasins are driven by translation

628 and viscous drag of a thick salt interval over complex base-salt relief and, thus, are

629 described as ramp-syncline basins (RSBs). Additionally, the occurrence of intra-

630 salt seaward-vergent shear zones (Figs. 6-11) supports our interpretation of

631 viscous salt drag (i.e. Couette flow) and basinward translation in the study-area.

632 An alternative hypothesis is that RSBs could be formed as expulsion rollovers as

633 the distinction between salt expulsion (i.e. Pouiseulle flow) and lateral (i.e. Couette)

634 flow in the generation of accommodation is a typical conundrum in salt tectonics

635 (Hossack, 1995; Jackson and Hudec, 2005; Jackson et al., 2014). Jackson and

636 Hudec (2005) have shown how discordant and stacked onlap surfaces that

637 become younger landward (Figs. 6-11) with common stratigraphic jumps across

638 diapirs (Figs. 9 and 11) as seen in our examples could not be driven by salt

639 expulsion. Thus, the hypothesis of RSBs on the SPP to have formed as expulsion

640 rollovers does not work.

641 7.2. Extensional vs. salt-related RSBs

642 Classical RSBs (Fig. 1a-b) are generated by regional extension, in which the

643 controlling fault cuts progressively downwards through pre-kinematic strata.

644 Consequently, the pre-kinematic interval appears both above and below the fault.

645 The basal boundary is, thus, defined by an extensional rollover composed of pre-

646 kinematic strata and a fault surface that is formed at the onset of translation, and

647 which maintains its original geometry through time (Fig. 1a-b). The pattern of

648 vertical movement of the hangingwall is controlled by the shape of the extensional

649 fault. As a consequence, the geometry and location of the subsiding minibasin

650 does not change as the system evolves, and the rate of subsidence is directly

651 proportional to the rate of lateral translation. Therefore, in an extensional RSB,

652 translation of the cover can result in subsidence, but not in uplift (Fig. 1a-b).

653 In contrast, salt-detached RSBs are not directly driven by extension. Instead, they

654 form by cover translation above salt (Fig. 1c-d), which, in turn, occurs in response

655 to gravity-driven extension updip, and is linked to contraction and/or salt advance

656　downdip (Jackson and Hudec, 2005; Jackson et al 2015). The basal slip surface is

657　stratabound, i.e. parallel to the pre-kinematic stratigraphy (Jackson and Hudec,

658　2005), so pre-kinematic strata always occur below their basal surface (Fig. 1c-d).

659　The base-salt relief is usually related to inherited topography due to previous

660　basement faulting (Davison et al. 2012); so translation and RSB development

661　occur after and are decoupled from pre-salt deformation.

662　Movement takes place by shearing of a slip volume (viscous salt) rather than a

663　discrete slip surface (extensional fault in classical RSBs) (Fig. 1c-d). Thus, salt

664　drag, expulsion and diapirism generate vertical movements, additional

665　accommodation, and complexities not observed in extensional systems. The shape

666　and size of the subsiding minibasin changes as the system evolves, because the

667　geometry and thickness of the salt detachment vary as the cover moves.

668　Additionally, as the RSB evolves with increasing displacement, vertical movement

669　of the surface may change from laterally variable subsidence, to subsidence plus

670　local uplift (Figs. 1c-d and 14-19).

671　**7.3. Controls on RSBs style: thick vs. thin salt RSBs**

672　In the Kwanza Basin, offshore Angola, RSBs formed by 23-26 km of salt-detached

673　translation over a major base-salt step (Atlantic Hinge Zone, fig. 20) (Peel et al.

674　1998, Hudec and Jackson, 2004, Jackson and Hudec, 2005; Peel 2014). These

675　RSBs consist of a synclinal wedge of growth strata that dips and expands landward

676　(E-ENE) towards a diachronous basal boundary that becomes younger and

677　steeper landward (Fig. 20). They are defined by a basinward-dipping axial trace

678 that also becomes steeper landward, with their updip edge occuring immediately

679 above a base-salt basinward-dipping ramp (Jackson and Hudec, 2005; Peel 2014).

680 Their geometry, stratigraphic architecture, and relationship with base-salt

681 topography are thus similar to the examples shown here from the Santos Basin

682 (Figs. 6-10).

683 RSBs on the SPP have a more complex stratigraphic architecture than those

684 offshore Angola, displaying pronounced folding and rotation of syn-kinematic strata

685 (Figs. 6-10), when compared to similar systems in the Kwanza Basin (Figs. 6-10

686 and 20). This difference can be explained by the stronger effects of synchronous to

687 post-depositional diapirism deforming and segmenting RSBs on the SPP, which, in

688 turn, are related to the differences in salt thickness between the two basins

689 (compare salt thickness between Figs. 3b and 20). More, specifically, in the

690 Kwanza Basin, RSBs are developed above a relatively thin (>1 km, Peel 2014),

691 and, now locally welded salt layer; with most diapirs already present at the onset of

692 translation (Jackson and Hudec, 2005). As a result, vertical salt movements and

693 diapirism during translation and generation of RSBs was limited.

694 Across the Atlantic, on the SPP, the RSBs occur above still thick (>2 km),

695 lithologically and rheologically layered salt. Pre-translation salt structures are rare,

696 with most diapirism occurring during translation and development of RSBs (Figs. 6-

697 11), during the post-Albian (Guerra and Underhill, 2012; Fiduk and Rowan, 2012;

698 Jackson et al. 2015). Layer-parallel shearing (i.e. Couette flow) within the salt was

699 aided by intra-salt layering that accommodated most of basinward flow along

700 multiple detachments and seaward-verging shear zones (Figs. 6-8). Sedimentation

within RSBs loaded the salt beneath them, expelling it and promoting diapirism (Figs. 9-11). Thus, synchronous diapirism was a more important control on the evolution of RSBs on the SPP than the ones in the Kwanza Basin, resulting in higher degree of folding, rotation, and localized erosion (Figs. 9-11), potentially and locally obscuring their original geometries.

Another important contrast between these two basins relates to the timing and rate of translation. In Kwanza, RSBs are capped at their landward edges by the seafloor, demonstrating translation is still ongoing (Fig. 20) (Jackson and Hudec, 2005). These authors estimate that RSB formation and, thus, translation, initiated in the Middle Miocene. If correct, this would correspond to a total translation time of 12-13 Myr and a relatively fast horizontal translation rate of 2 mm/year, 2-4 times higher than the typical deformation rates encountered in salt-detached, gravity-driven systems (Rowan et al. 2004).

On the SPP, translation and RSB generation started at the end of the Albian and stopped during the middle Paleocene (Figs. 7-11). Horizontal translation magnitude varied from 28-32 km, yielding an approximate rate of 0.7–0.8 mm/year; this is also relatively fast, but comparable to rates estimated from the Gulf of Mexico (0.1–0. 5 mm/yr) and the Kwanza Basin (0.4-0.5 mm/yr) (Rowan et al. 2000; 2004). In summary, although, the amount and pattern of horizontal translation between the two basins is remarkably similar, the timing and rate are significantly different. We still do not fully understand why these contrasts arise but, due to the nature of the 2D data and the limited well-control from the earlier work of Jackson and Hudec

723 (2005), we speculate their estimate of when translation began in the Kwanza Basin

724 could be inaccurate.

725 A relatively recent study by Dooley et al. (2016) documents a RSB from the

726 Campos Basin, Brazil. Here, translation started at the end of the Albian, which is

727 consistent with what we observe further SW in the Santos Basin. As the Kwanza

728 Basin corresponds to the conjugate margin of Campos and Espirito-Santo basins

729 (Lentini et al., 2010; Jackson and Hudec, 2017), it is probable that both margins

730 experienced similar early histories and, thus, translation started earlier than

731 originally estimated by Jackson and Hudec (2005). Deciding why translation is still

732 ongoing in the Kwanza Basin and stopped in the Santos Basin is outside of the

733 scope of this study, as this would require a more regional analysis involving

734 transects comprising the whole extent of both margins. Nevertheless, we may

735 speculate that the following led to this key difference: 1) the mobile halite-

736 dominated interval, represented by the lowermost transparent seismic facies within

737 the salt, thinned dramatically in between diapirs in the SPP (Figs. 7-10), reducing

738 the overall mobility of the system; 2) late dip-reversal of the basal detachment due

739 to significant sedimentary loading associated with formation of the Albian Gap,

740 landward of the SPP (Fig. 3 and 7) (Davison et al. 2012); and 3) progressive

741 basinward translation allowed the system to reach the downdip contractional

742 domain (Fig.3b).

743 **7.4. Occurrence of RSBs in other salt basins**

744 There are currently very few publications describing salt-related RSBs. Apart from

745 Rowan (2014) and Dooley et al. (2016), who briefly describe RSBs in the Red Sea

746 and Campos Basin, respectively, all others previous studies refer exclusively to

747 RSBs in the Kwanza Basin, (Marton et al. 1998, Peel et al. 1998; Jackson and

748 Hudec, 2005). The question that remains is: "how widespread are salt-related

749 RSBs?".

750 We believe that because of: (i) their unique and complex stratigraphic architecture,

751 (ii) the lack of a detailed 3D subsurface or outcrop analysis, (iii) physical and

752 numerical modelling of these features, and (iv) because they are commonly

753 affected by other salt tectonic processes, RSBs have been previously overlooked.

754 As an example of their occurrence in other salt basins, we present a 2D seismic

755 profile through a RSB formed above allochthonous salt in the Essaouira-Agadir

756 Basin, offshore Morocco (Fig. 21).

757 In the western portion of the section, there is a clear example of a RSB formed

758 above thick (~1 km) allochthonous salt. This RSB is underlain by a basinward-

759 dipping ramp at its base. The RSB is characterized by asymmetric and gently

760 folded strata thickening and dipping mainly landward towards a diachronous

761 basinward-dipping onlap surface. The system is defined by a steep, basinward-

762 dipping axial trace and onlap stratal terminations that grade upward into transitional

763 boundaries (Fig. 21), a geometry characteristic of systems with relative high $\square/\square$.

764 Total translation recorded is 9.4 km during Paleocene to Pliocene times, equivalent

765 to rates of 0.15-0.2 mm/year, and comparable with previous estimates of salt

766 translation rates (Rowan et al. 2004). The RSB is bounded updip by an extensional

767 domain with normal faults and an extensional rollover, and downdip by an inflated

768 salt tongue that was formed early by open-toe advance, being subsequently

769 buried, folding and uplifting its roof (Fig. 21). There is also another potential

770 candidate for an RSB occurring further updip but the seismic data quality in this

771 part of the section renders the interpretation of the updip RSB and its causal ramp

772 somewhat speculative.

773 **8.   Conclusion**

774 We use 3D seismic reflection data to describe the geometry and tectono-

775 stratigraphic development of salt-detached RSBs formed above thick (> 2 km) salt

776 in the São Paulo Plateau, Santos Basin, Brazil. We compared our observations

777 from this natural system to results of forward models simulating cover translation

778 and viscous salt drag above variable base-salt topography; this allowed us to

779 analyse the kinematics and sequential evolution of RSBs and, explain their

780 geometries and relationship with base-salt topography.

781 On the SPP, RSBs show consistent magnitudes of total translation, varying from

782 28 to 32 km, and movement direction, which varies from ESE to SE. We have

783 demonstrated these systems have similar geometries, stratigraphic architecture,

784 and relationship to base-salt steps to previously published examples from the

785 Kwanza Basin, offshore Angola (Jackson and Hudec, 2005, Peel 2014). However,

786 on the SPP, ramp-syncline basins are generally more complex because they occur

787 above thick salt and, consequently, are more affected by synchronous diapirism

788 and salt-related deformation. We have also demonstrated that cover translation

789 above landward-dipping ramps can generate notably similar stratal geometries to

790 classical examples of RSBs formed above basinward-dipping ramps.

791 Our from seismic examples and models demonstrate there is a direct relationship

792 between RSB evolution and base-salt topography, as RSBs terminate updip

793 above the top of base-salt ramps, or above diapirs formed over the ramp. Thus,

794 mapping of RSBs can aid the identification of pre-salt structures, which may be

795 useful when exploring for hydrocarbons in areas of limited sub-salt seismic

796 reflection imaging quality when exploring for sub/pre-salt exploration targets.

797 Ultimately, this study improves our current knowledge of RSBs, working as a guide

798 for seismic interpretation and recognition of these systems in other salt basins

799 around the world.

Acknowledgements

References

811 Alves, T. M., Fetter, M., Lima, C., Cartwright, J. A., Cosgrove, J, Gangá, A, &

812 Strugale, M. (2017). An incomplete correlation between pre-salt topography, top

813 reservoir erosion, and salt deformation in deep-water Santos Basin (SE

814 Brazil). *Marine and Petroleum Geology*, *79*, 300-320.

815 Barton, N., 2007. Rock quality, seismic velocity, attenuation and anisotropy. CRC

816 press.

817 Benedicto, A., Séguret, M., & Labaume, P. (1999). Interaction between faulting,

818 drainage and sedimentation in extensional hanging-wall syncline basins: Example

819 of the Oligocene Matelles basin (Gulf of Lion rifted margin, SE France). *Geological*

820 *Society, London, Special Publications*, *156*(1), 81-108.

821 Carminatti, M., Wolff, B. & Gamboa, L. (2008). New exploratory frontiers in Brazil.

822 In 19th World Petroleum Congress. World Petroleum Congress.

823 Contreras, J., Zühlke, R., Bowman, S., & Bechstädt, T. (2010). Seismic

824 stratigraphy and subsidence analysis of the southern Brazilian margin (Campos,

825 Santos and Pelotas basins). *Marine and Petroleum Geology*, *27*(9), 1952-1980.

826 Cobbold, P. R., Szatmari, P., Demercian, L. S., Coelho, D., & Rossello, E. A.

827 (1995). Seismic and experimental evidence for thin-skinned horizontal shortening

828 by convergent radial gliding on evaporites, deep-water Santos Basin, Brazil. *In:*

829 Jackson, M. P. A., Roberts, D. G., Snelson, S. (eds) *Salt tectonics: a global*

830 *perspective.* AAPG Memoir 65, 305-321.

831   Demercian, S., Szatmari, P., & Cobbold, P. R. (1993). Style and pattern of salt
832   diapirs due to thin-skinned gravitational gliding, Campos and Santos basins,
833   offshore Brazil. *Tectonophysics*, *228*(3-4), 393-433.

834   Duval, B., Cramez, C., & Jackson, M. P. A. (1992). Raft tectonics in the Kwanza
835   basin, Angola. *Marine and Petroleum Geology*, *9*(4), 389-404.

836   Ellis, P. G., & McClay, K. R. (1988). Listric extensional fault systems-results of
837   analogue model experiments. *Basin Research*, *1*(1), 55-70.

838   Davison, I., Anderson, L., & Nuttall, P. (2012). Salt deposition, loading and gravity
839   drainage in the Campos and Santos salt basins. *Geological Society of London*
840   *Special Publications*, *363*(1), 159-174.

841   Dooley, T. P., Jackson, M. P., Jackson, C. A. L., Hudec, M. R., & Rodriguez, C. R.
842   (2015). Enigmatic structures within salt walls of the Santos Basin—Part 2:
843   Mechanical explanation from physical modelling. *Journal of Structural Geology*, *75*,
844   163-187.

845   Dooley, T. P., Hudec, M. R., Carruthers, D., Jackson, M. P., & Luo, G. (2016). The
846   effects of base-salt relief on salt flow and suprasalt deformation patterns—Part 1:
847   Flow across simple steps in the base of salt. *Interpretation*, *5*(1), SD1-SD23.

848   Fiduk, J. C., & Rowan, M. G. (2012). Analysis of folding and deformation within
849   layered evaporites in Blocks BM-S-8 &-9, Santos Basin, Brazil. *Geological Society,*
850   *London, Special Publications*, *363*(1), 471-487.

851 Gamboa, L.A.P., Machado, M.A.P., Silveira, D.P., Freitas, J.T.R. & Silva, S.R.P.,

852 2009. Evaporitos estratificados no Atlântico Sul: interpretação sísmica e controle

853 tectono-estratigráfico na Bacia de Santos. In: W. Mohriak, P. Szatmari & S. M. C.

854 Anjos (Org.), Sal: Geologia e Tectônica. Editora Beca, São Paulo, 2ed., p. 343-

855 361.

856 Ge, H., Jackson, M. P., & Vendeville, B. C. (1997). Kinematics and dynamics of

857 salt tectonics driven by progradation. *AAPG bulletin, 81*(3), 398-423.

858 Gemmer, L., Ings, S.J., Medvedev, S. and Beaumont, C. (2004). Salt tectonics

859 driven by differential sediment loading: stability analysis and finite-element

860 experiments. *Basin Research*, *16*(2), 199-218.

861 Gibbs, A. D. (1984). Structural evolution of extensional basin margins. *Journal of*

862 *the Geological Society*, *141*(4), 609-620.

863 Guerra, M. C., & Underhill, J. R. (2012). Role of halokinesis in controlling structural

864 styles and sediment dispersal in the Santos Basin, offshore Brazil. *Geological*

865 *Society, London, Special Publications*, *363*(1), 175-206.

866 Flinch, J., 2014. Context, challenges, and future of deep-water plays: an overview.

867 Search and Discovery Article, 41417.

868 Gemmer, L., Ings, S. J., Medvedev, S., Beaumont, C., 2004. Salt tectonics driven

869 by differential sediment loading: stability analysis and finite-element

870 experiments. Basin Research, 16(2), 199-218.

871 Gomes, P.O., Kilsdonk, B., Grow, T., Minken, J. & Barragan, R. (2012). Tectonic

872 evolution of the outer high of Santos basin, southern São Paulo Plateau, Brazil,

873 and implications for hydrocarbon exploration. *In*: Gao, D. (eds) *Tectonics and*

874 *Sedimentation: Implications for Petroleum Systems*. AAPG Memoir 100, 125–142.

875 Gradmann, S., Beaumont, C., 2016. Numerical modelling study of mechanisms of

876 mid-basin salt canopy evolution and their potential applications to the Northwestern

877 Gulf of Mexico. Basin Research.

878 Hudec, M. R. & Jackson, M. P. A. (2004). Regional restoration across the Kwanza

879 Basin, Angola: Salt tectonics triggered by repeated uplift of a metastable passive

880 margin. *AAPG bulletin*, *88*(7), 971-990.

881 Hossack, J., 1995. Geometric rules of section balancing for salt structures. In:

882 Jackson, M.P.A., Roberts, D.G., Snelson, S. (Eds.), Salt Tectonics: a Global

883 Perspective American Association of Petroleum Geologists Memoir, 65, pp. 29–40.

884 Jackson, M. P. A. & Cramez, C. (1989). Seismic recognition of salt welds in salt

885 tectonics regimes. *In: Gulf of Mexico salt tectonics, associated processes and*

886 *exploration potential: Gulf Coast Section SEPM Foundation 10th Annual Research*

887 *Conference*, 66-71.

888 Jackson, M. P. A., Hudec, M. R., Fraenkl, R., Sikkema, W., Binga, L. & Da Silva, J.

889 (2001). Minibasins translating down a basement ramp in the deepwater monocline

890 province of the Kwanza Basin, Angola [abs.]. *In*: *American Association of*

891 *Petroleum Geologists Annual Meeting Official Program*, *10*, A99.

892 Jackson, M.P. & Hudec, M.R. (2017). Salt Tectonics: Principles and Practice.
893 Cambridge University Press.

894 Jackson, M. P., & Hudec, M. R. (2005). Stratigraphic record of translation down
895 ramps in a passive-margin salt detachment. *Journal of Structural Geology*, *27*(5),
896 889-911.

897 Jackson, C. A. L., Jackson, M. P., & Hudec, M. R. (2015). Understanding the
898 kinematics of salt-bearing passive margins: A critical test of competing hypotheses
899 for the origin of the Albian Gap, Santos Basin, offshore Brazil. *Geological Society*
900 *of America Bulletin*, *127*(11-12), 1730-1751.

901 Jackson, C. A. L., Rodriguez, C. R., Rotevatn, A., & Bell, R. E. (2014). Geological
902 and geophysical expression of a primary salt weld: An example from the Santos
903 Basin, Brazil. *Interpretation*, *2*(4), SM77-SM89.

904 Jackson, C. A. L., Jackson, M. P., Hudec, M. R., & Rodriguez, C. R. (2015).
905 Enigmatic structures within salt walls of the Santos Basin—Part 1: Geometry and
906 kinematics from 3D seismic reflection and well data. *Journal of Structural*
907 *Geology*, *75*, 135-162.

908 Jones, I. F., & Davison, I. (2014). Seismic imaging in and around salt
909 bodies. *Interpretation*, *2*(4), SL1-SL20.

910 Karner, G. D., & Gambôa, L. A. P. (2007). Timing and origin of the South Atlantic
911 pre-salt sag basins and their capping evaporites. *Geological Society, London,*
912 *Special Publications*, *285*(1), 15-35.

913 Lentini, M. R., Fraser, S. I., Sumner, H. S., & Davies, R. J. (2010). Geodynamics of

914 the central South Atlantic conjugate margins: implications for hydrocarbon

915 potential. Petroleum Geoscience, 16(3), 217-229.

916 Marton, G., Tari, G. & Lehmann, C. (1998) Evolution of salt-related structures and

917 their impact on the post-salt petroleum systems of the Lower Congo Basin,

918 offshore Angola. *In*: American Association of Petroleum Geologists International

919 Conference and Exhibition, Rio de Janeiro. Extended Abstracts Volume, 834–834.

920 Marton, G., Tari, G. & Lehmann, C. (2000). Evolution of the Angolan Passive

921 Margin, West Africa, With Emphasis on Post-Salt Structural Styles. *Atlantic rifts*

922 *and continental margins*, 129-149.

923 McClay, K. R. (1990). Extensional fault systems in sedimentary basins: a review of

924 analogue model studies. *Marine and petroleum Geology*, *7*(3), 206-233.

925 McClay, K. R., & Scott, A. D. (1991). Experimental models of hangingwall

926 deformation in ramp-flat listric extensional fault systems. *Tectonophysics*, *188*(1-2),

927 85-96.

928 McClay, K. R. (1996). Recent advances in analogue modelling: uses in section

929 interpretation and validation. *Geological Society, London, Special*

930 *Publications*, *99*(1), 201-225.

931 Meisling, K. E., Cobbold, P. R., & Mount, V. S. (2001). Segmentation of an

932 obliquely rifted margin, Campos and Santos basins, southeastern Brazil. *AAPG*

933 *bulletin*, *85*(11), 1903-1924.

934   Modica, C. J., & Brush, E. R. (2004). Postrift sequence stratigraphy,
935   paleogeography, and fill history of the deep-water Santos Basin, offshore
936   southeast Brazil. *AAPG bulletin*, *88*(7), 923-945.

937   Mohriak, W.U., Macedo, J.M., Castellani, R.T., Rangel, H.D., Barros, A.Z.N., Latgé,
938   M.A.L., Mizusaki, A.M.P., Szatmari, P., Demercian, L.S., Rizzo, J.G. & Aires, J.R.
939   (1995). Salt tectonics and structural styles in the deep-water province of the Cabo
940   Frio region, Rio de Janeiro, Brazil. *In:* Jackson, M. P. A., Roberts, D. G., Snelson,
941   S. (eds) *Salt tectonics: a global perspective.* AAPG Memoir 65, 273-304.

942   Mohriak, W., Nemčok, M., & Enciso, G. (2008). South Atlantic divergent margin
943   evolution: rift-border uplift and salt tectonics in the basins of SE Brazil. *Geological*
944   *Society, London, Special Publications*, *294*(1), 365-398.

945   Mohriak, W.U., Szatmari, P., Anjos, S.M.C., 2008. Sal: Geologia e Tectônica.
946   Editora Beca, São Paulo,450 pp

947   Mohriak, W. U., Szatmari, P., & Anjos, S. (2012). Salt: geology and tectonics of
948   selected Brazilian basins in their global context. *Geological Society, London,*
949   *Special Publications*, *363*(1), 131-158.

950   Mohriak, W. (2015). Pre-Salt Carbonate Reservoirs in the South Atlantic and
951   World-wide Analogs. In AAPG Geosciences Technology Workshop "Carbonate
952   Plays around the World-Analogues to Support Exploration and Development (pp.
953   4-5).

954 Osmundsen, P. T., Bakke, B., Svendby, A. K., & Andersen, T. B. (2000).
955 Architecture of the Middle Devonian Kvamshesten Group, western Norway:
956 sedimentary response to deformation above a ramp-flat extensional
957 fault. *Geological Society, London, Special Publications*, *180*(1), 503-535.

958 Peel, F., Jackson, M.P. & Ormerod, D. (1998) Influence of Major Steps in the Base
959 of Salt on the Structural Style of Overlying Thin-skinned Structures in Deep Water
960 Angola, American Association of Petroleum Geologists International Conference
961 and Exhibition, Rio de Janeiro, Brazil, November, Extended Abstracts Volume, pp.
962 366-367.

963 Peel, F. J. (2014). The engines of gravity-driven movement on passive margins:
964 Quantifying the relative contribution of spreading vs. gravity sliding
965 mechanisms. *Tectonophysics*, *633*, 126-142.

966 Pichel, Leonardo M., Emma Finch, Mads Huuse, and Jonathan Redfern. "The
967 influence of shortening and sedimentation on rejuvenation of salt diapirs: A new
968 Discrete-Element Modelling approach." Journal of Structural Geology 104 (2017):
969 61-79.

970 Quirk, D. G., Schødt, N., Lassen, B., Ings, S. J., Hsu, D., Hirsch, K. K., & Von
971 Nicolai, C. (2012). Salt tectonics on passive margins: examples from Santos,
972 Campos and Kwanza basins. *Geological Society, London, Special*
973 *Publications*, *363*(1), 207-244.

974 Rowan, M. G., Jackson, M. P., & Trudgill, B. D. (1999). Salt-related fault families
975 and fault welds in the northern Gulf of Mexico. *AAPG bulletin*, *83*(9), 1454-1484.

976 Rowan, M. G., Peel, F. J., & Vendeville, B. C. (2004). Gravity-driven fold belts on
977 passive margins.

978 Rowan, M. G., 2004, Do salt welds seal?: Presented at GCSSEPM Foundation
979 24th Annual Bob F. Perkins Research Conference, 390–403.

980 Rowan, M.G., 2014. Passive-margin salt basins: hyperextension, evaporite
981 deposition, and salt tectonics. *Basin Research*, *26*(1), 154-182.

982 Sanchis, E. & Séranne, M. (2000). Structural style and tectonic evolution of a
983 polyphase extensional basin of the Gulf of Lion passive margin: the Tertiary Ales
984 basin, southern France. *Tectonophysics*, *322*(3), 219-242.

985 Schuster, D. C. (1995). Deformation of allochthonous salt and evolution of related
986 salt-structural systems, eastern Louisiana Gulf Coast. *In:* Jackson, M. P. A.,
987 Roberts, D.G., Snelson, S. (Eds.), Salt Tectonics: a Global Perspective. AAPG
988 Memoir, vol. 65, pp. 177–198.

989 Roberts, D. G., Snelson, S. (eds) *Salt tectonics: a global perspective.* AAPG
990 Memoir 65, 177-198.

991 Tari, G., & Jabour, H. (2013). Salt tectonics along the Atlantic margin of
992 Morocco. *Geological Society, London, Special Publications*, *369*(1), 337-353.

993 Weijermars, R., Jackson, M. T., & Vendeville, B. (1993). Rheological and tectonic
994 modeling of salt provinces. *Tectonophysics*, *217*(1-2), 143-174.

995   Weijermars, R., Hudec, M. R., Dooley, T. P., & Jackson, M. P. A., 2015.

996   Downbuilding salt stocks and sheets quantified in 3-D analytical models. Journal of

997   Geophysical Research: Solid Earth, 120(6), 4616-4644.
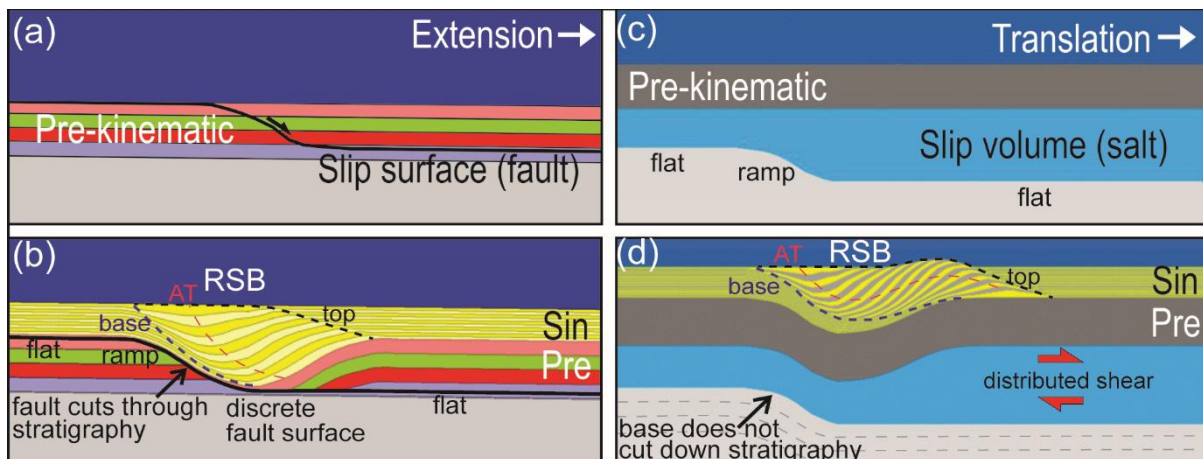
Figure 1: Models of RSB development. (a-b) represent "classic" RSBs (McClay, 1990, 1996; Benedicto et al., 1999), with (a) illustrating the system prior to deformation, and (b), the system during extension with development of a RSB characterized by an asymmetric depocentre with basinward-dipping axial trace (AT) above a discrete extensional fault that cuts down through stratigraphy in a ramp-flat trajectory. Movement of the hanging-wall creates differential amounts of subsidence and as long as the fault is extensional, there is no hanging-wall uplift. This contrasts with the model for salt-detached RSBs shown in (c-d). The process is not extensional; instead the RSB forms by translation of the cover over a viscous salt layer. A downward offset of the base of salt takes the place of the fault ramp. The offset does not cut down through stratigraphy. Shear strain is distributed through the viscous salt and results in uplift on the downdip side of salt-detached RSBs. The base and top boundaries of the RSBs are diachronous, and consist either of onlap/offlap unconformity surfaces, or regions of abrupt stratal thinning.
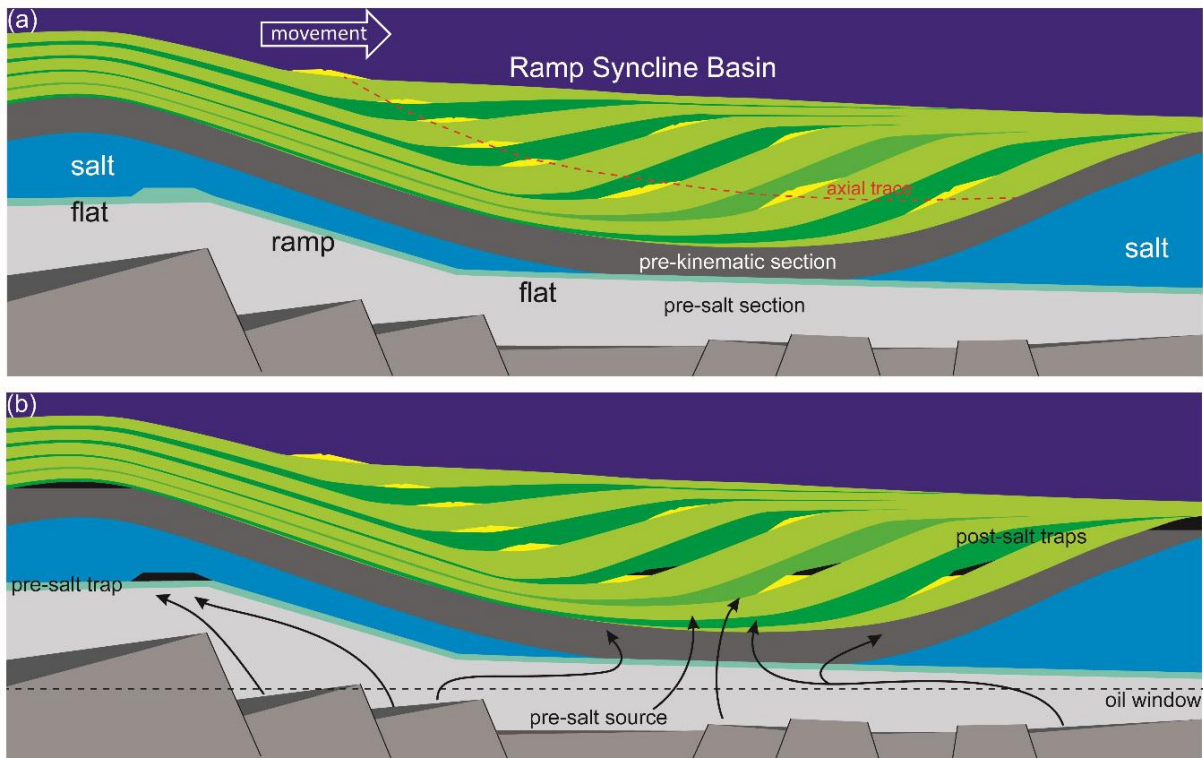
Figure 2: Schematic cross-sections: (a) illustrating typical geometry of simple RSBs formed above salt-detachments with a basinward-dipping ramp; and (b) displaying potential hydrocarbon plays that can be associated with RSBs in these settings: pre-salt carbonates (blueish green) occurring at the top of the pre-salt ramps and below the updip limit of the RSBs (e.g. Tupi and Iracema discoveries); carbonates on the crest of salt anticlines, and supra-salt sandier intervals juxtaposed above deeper and mature pre-salt source rocks, which can be charged with salt welding below the RSB.
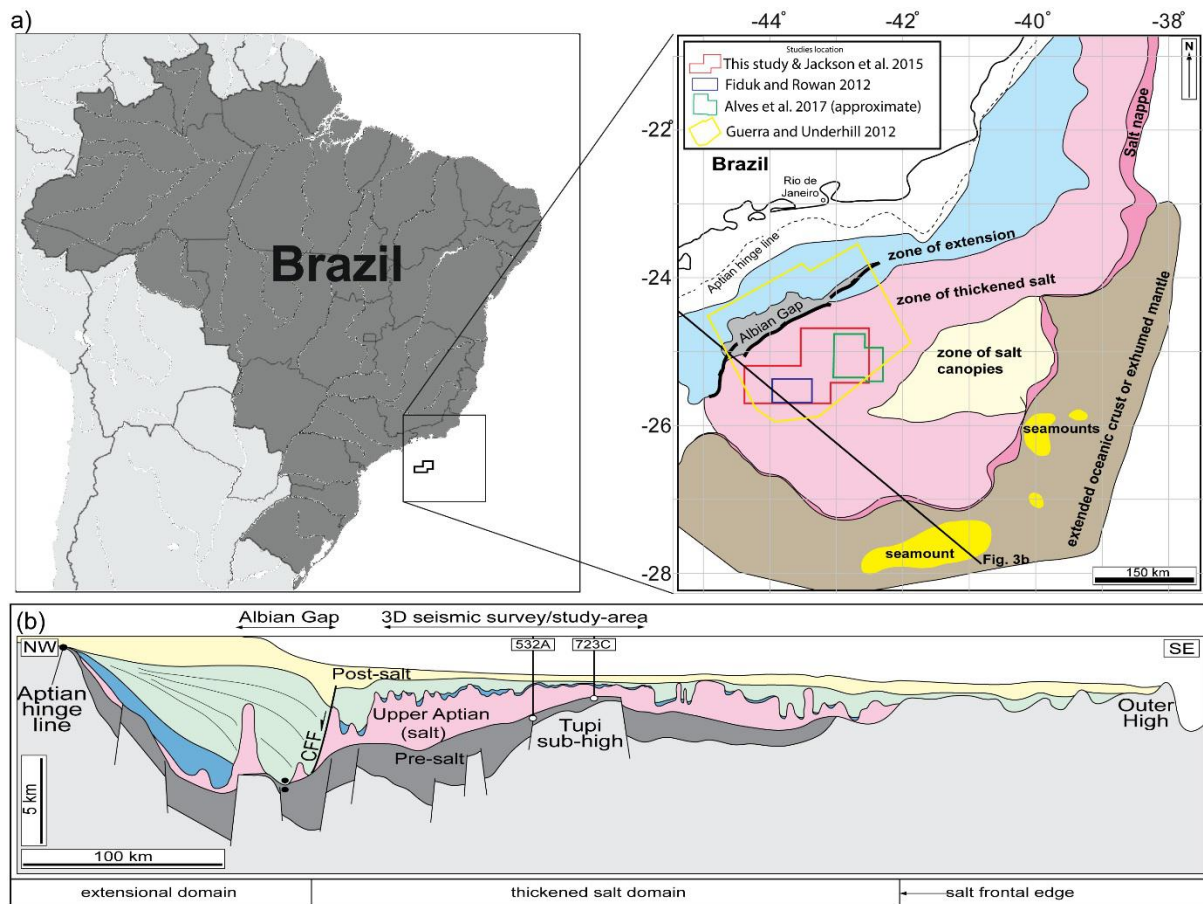
Figure 3: (a) Location map showing the 3D dataset and study-area (Jackson et al. 2015) in its regional context and datasets presented in earlier studies. (b) Simplified geoseismic section across the central Santos Basin illustrating basement structures and salt-related structural provinces. CFF refers to the Cabo Frio "Fault" (Guerra and Underhill, 2012). Vertical exaggeration of cross-section is 20:1 and location is shown in (a).
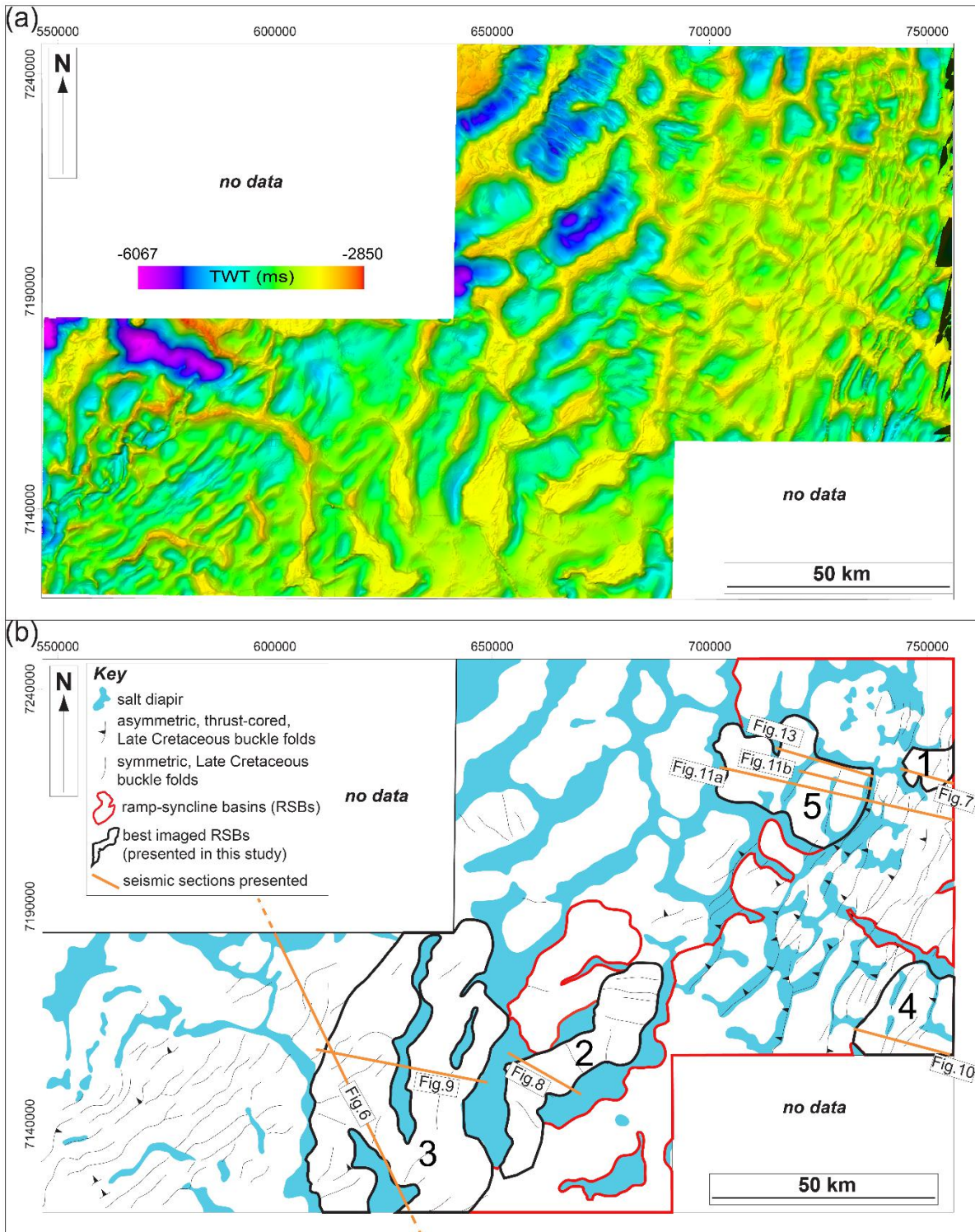
Figure 4: (a) Top-salt map showing complex pattern of salt walls and stocks. (b) Drawn top-salt map with main structures (adapted from Jackson et al. 2015), and distribution of RSBs. The examples presented in this study are in black polygons (RSB 1-5).
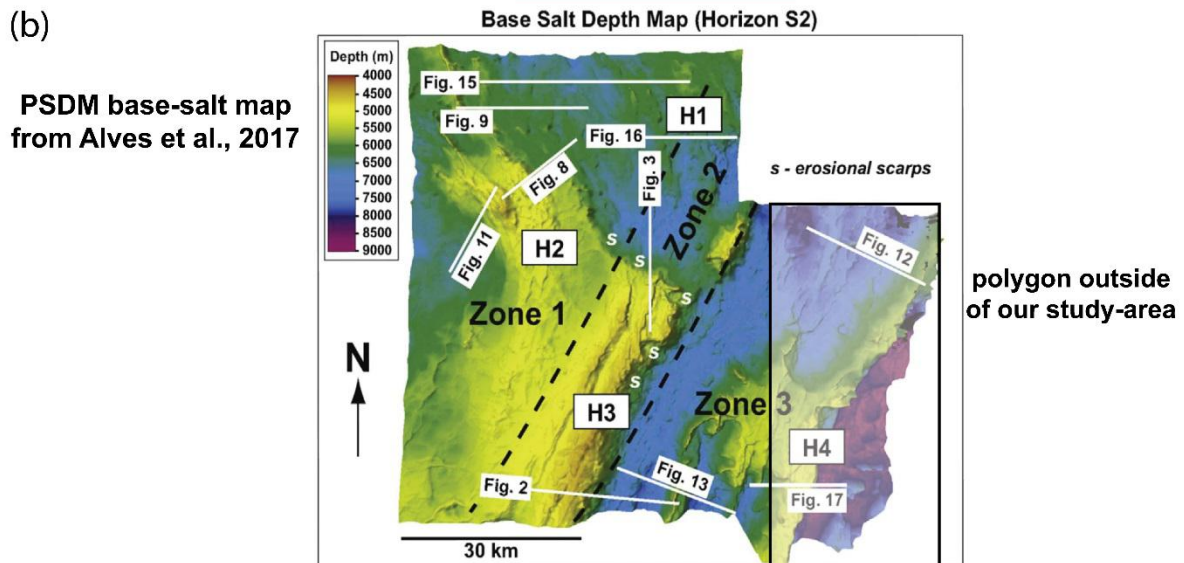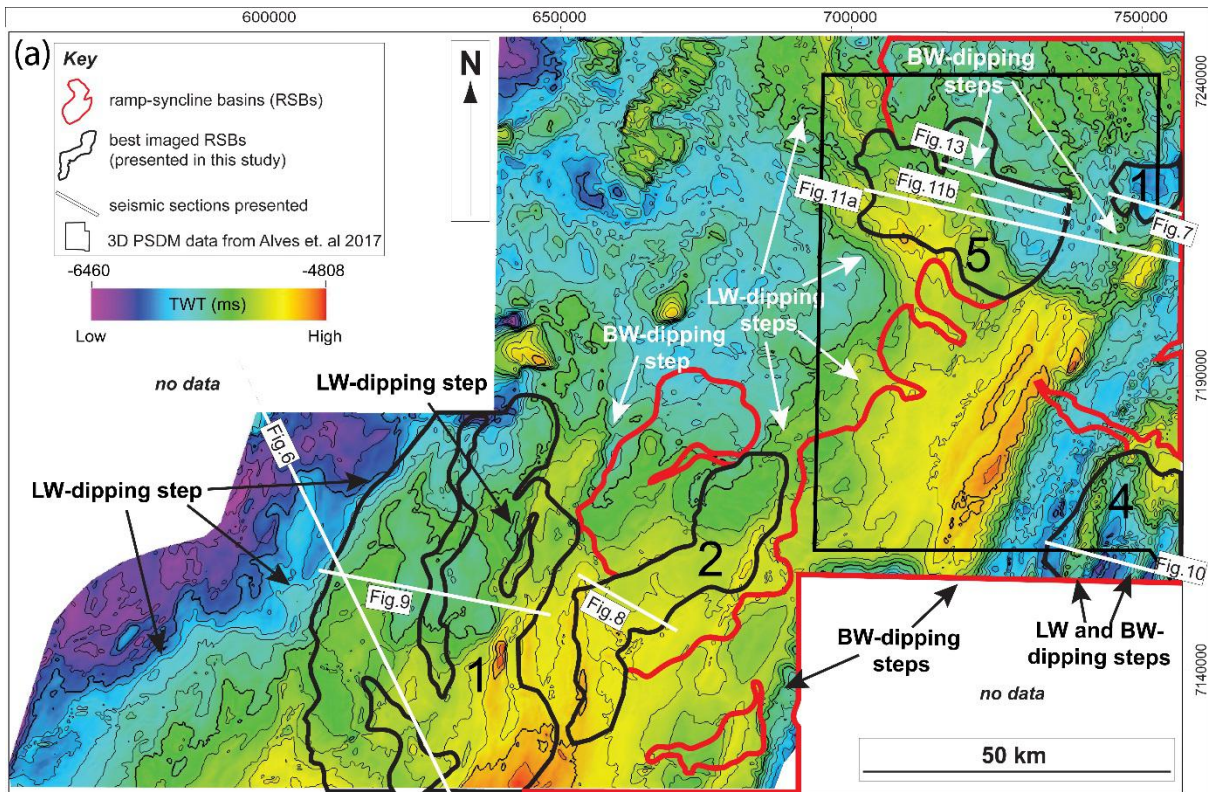
Figure 5: (a) Static-corrected base-salt map showing the largest base-salt highs and steps in the area. They are indicated on map with arrows and trend predominantly NNE-NE, although the northernmost high (beneath RSB 5) trends NNW. Map shows that the RSBs (red and black polygons) are distributed above and/or basinward of these base-salt structures. (b) Base-salt map extracted from 3D PSDM data from Alves et al., 2017, comprising part of our study-area and showing the same pre-salt main structures.
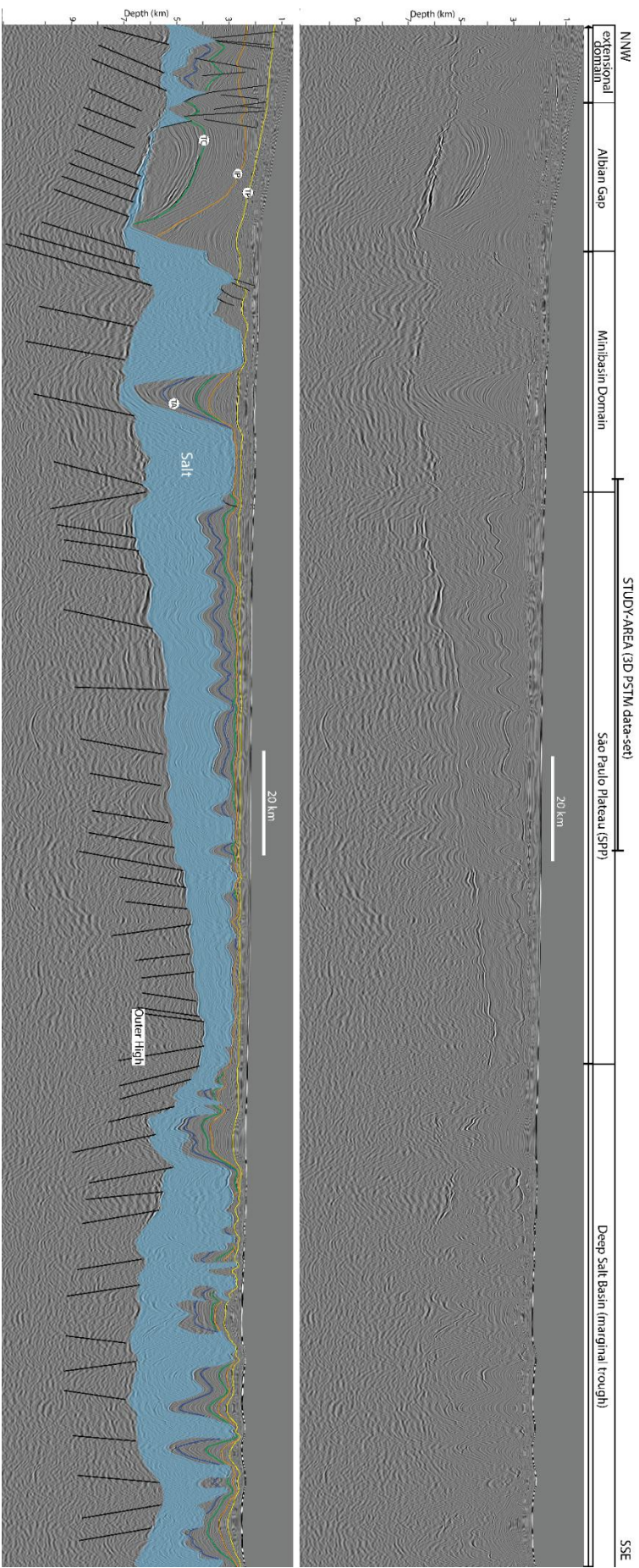
Figure 6: Uninterpreted and interpreted PSDM transect of the Central Santos salt basin comprising the updip extensional domain, Albian Gap, São Paulo Plateau (SPP) and the deep salt basin (marginal trough). The section illustrates the regional salt (light blue) structural styles and overall base-salt geometry characterized by multiple base-salt ramps and having 0.5-2 km of structural relief and dipping either basin- or landward in the study-area. The Albian (dark-blue horizon) is broadly tabular in the study-area, whereas the Late Cretaceous-Paleocene section shows stronger thickness variations and asymmetric growth strata defined by predominantly landward-dipping and thicknening section. Main faults in black and key-horizons are: top-Albian (TA, dark-blue), top-Cretaceous (TC, green), Intra-Paleocene unconformity (orange, IP) and top-Paleocene (yellow).
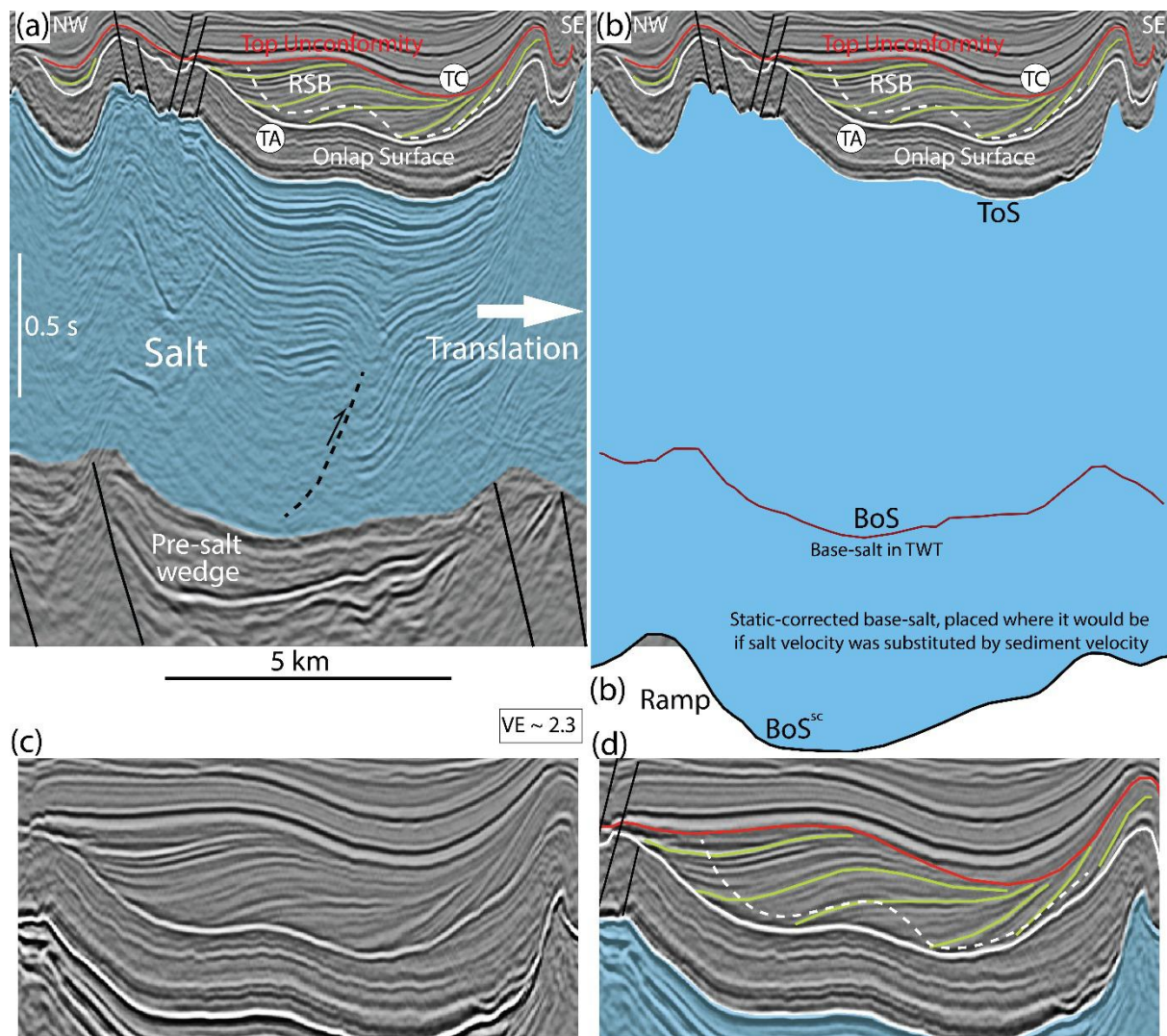
Figure 7: (a) Interpreted seismic section of RSB 1 with salt in blue and faults in black. Top Albian (TA) and top Cretaceous (TC) horizons based on Jackson et al. 2015. RSB characterized by landward-dipping and thickening sigmoidal strata (green) above an onlap surface (white, top Albian) and capped by a diachronous unconformity (red) that finishes updip at top Cretaceous. RSB axial trace (dashed red) steepens landward. Intra-salt seaward-vergent shear zones (black dashed lines) indicate lateral movement and viscous salt drag. Pre-salt wedges and faults are used as a cross-check of the static-corrected base-salt map and base-salt structures. In (b), the relationship between the RSB and base-salt structure is presented through the static-corrected base-salt (BoS^{sc}) which shows that the RSB landward edge occurs above the top of a base-salt basinward-dipping ramp. Uninterpreted (c) and interpreted (d) zooms of the RSB section show in detail its tectono-stratigraphic architecture and key-surfaces. For a complete uninterpreted section, see supplementary material.

(a)

NW · SE

Minimum Translation = 18 km

Top Unconformity

RSB

Onlap Surface

0.5 s

Salt

5 km

Pre-salt wedges

VE ~ 2.3

(b)

NW · SE

Minimum Translation = 18 km

TP

IP

Top Unconformity

RSB

TC

Onlap Surface

TA

ToS

Salt

pull-ups removed

BoS

BoS^sc

Ramp

0.3 s

VE ~ 2.3

(c)

NW · SE

(d)

NW · SE
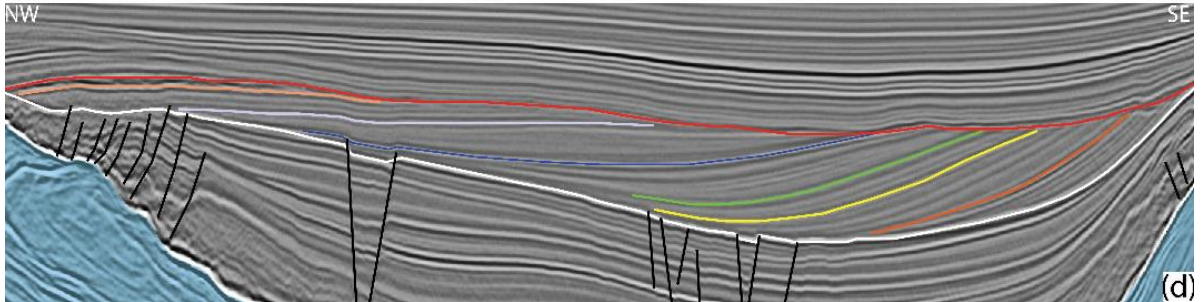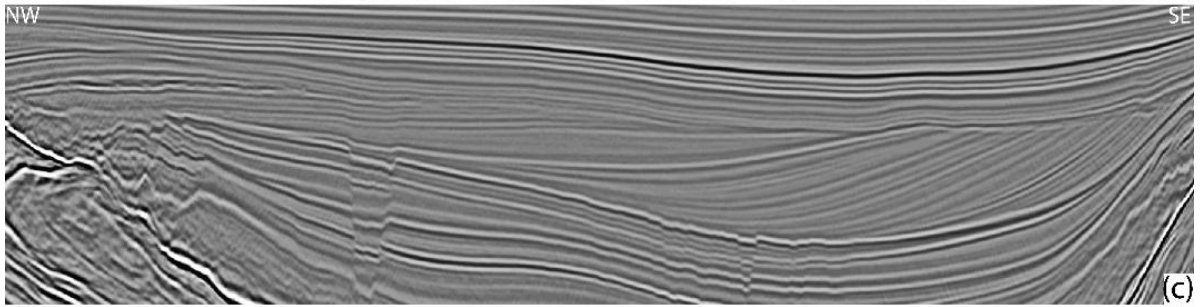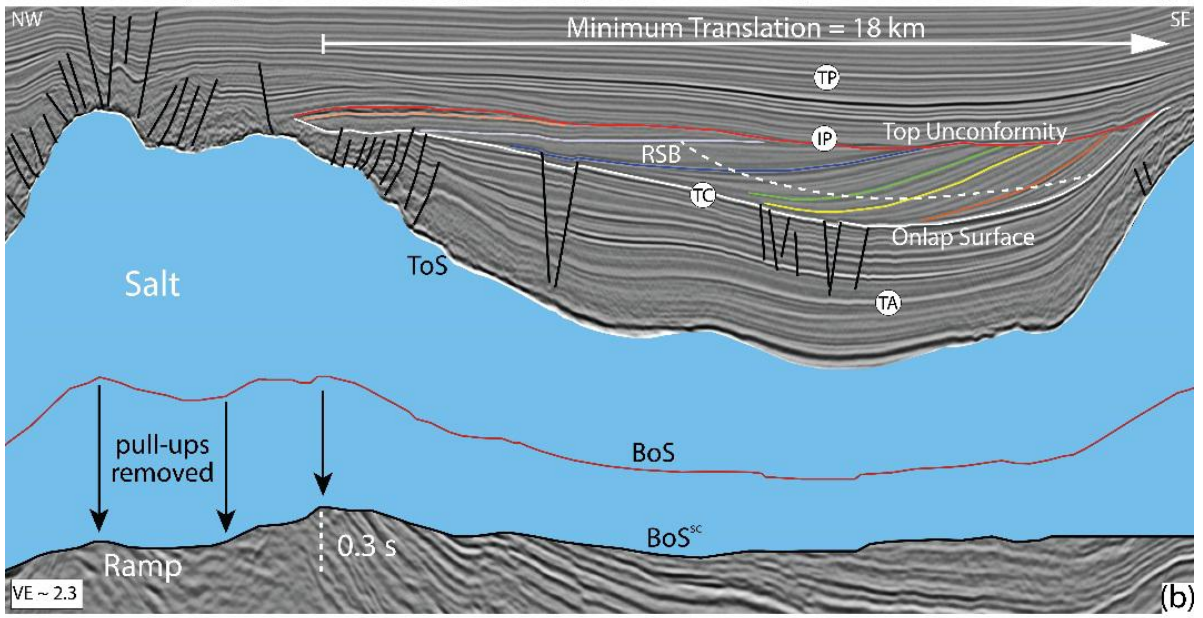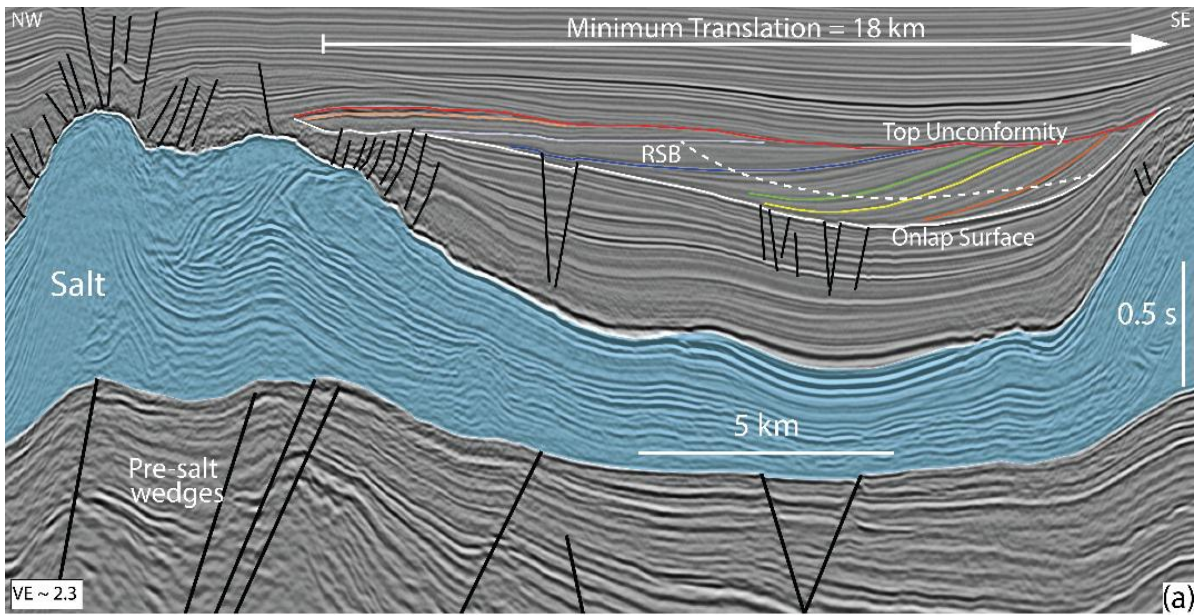
Figure 8: Seismic sections of the landward segment of RSB 2. Key horizons based on Jackson et al. 2015 are presented: top Albian (TA), top Cretaceous (TC), intra-Paleocene unconformity (IP) and top Paleocene (TP). In (a), interpretation of RSB 2, characterized by a well-defined onlap surface (white, TC) being onlapped by landward-dipping and thickening strata (colored lines), defined by a landward-steepening axial-trace (dashed red) and capped by the intra-Paleocene unconformity (red). Faults are in black. Pre-salt wedges and faults are used as a cross-check of static-corrected base-salt map and base-salt structures. Base-salt structural relief is shown with TWT values in dashed-white lines below base-salt. In (b), the RSB is presented in the context of the static-corrected base-salt (BoS^{sc}) to illustrate that the RSB finishes updip above a base-salt landward-dipping ramp, being surrounded by diapirs. Minimum translation of 18 km is measured from first landward onlap point within the RSB to the top of the ramp. Uninterpreted (c) and interpreted (d) zooms of RSB section are also shown. For a complete uninterpreted section, see supplementary material.
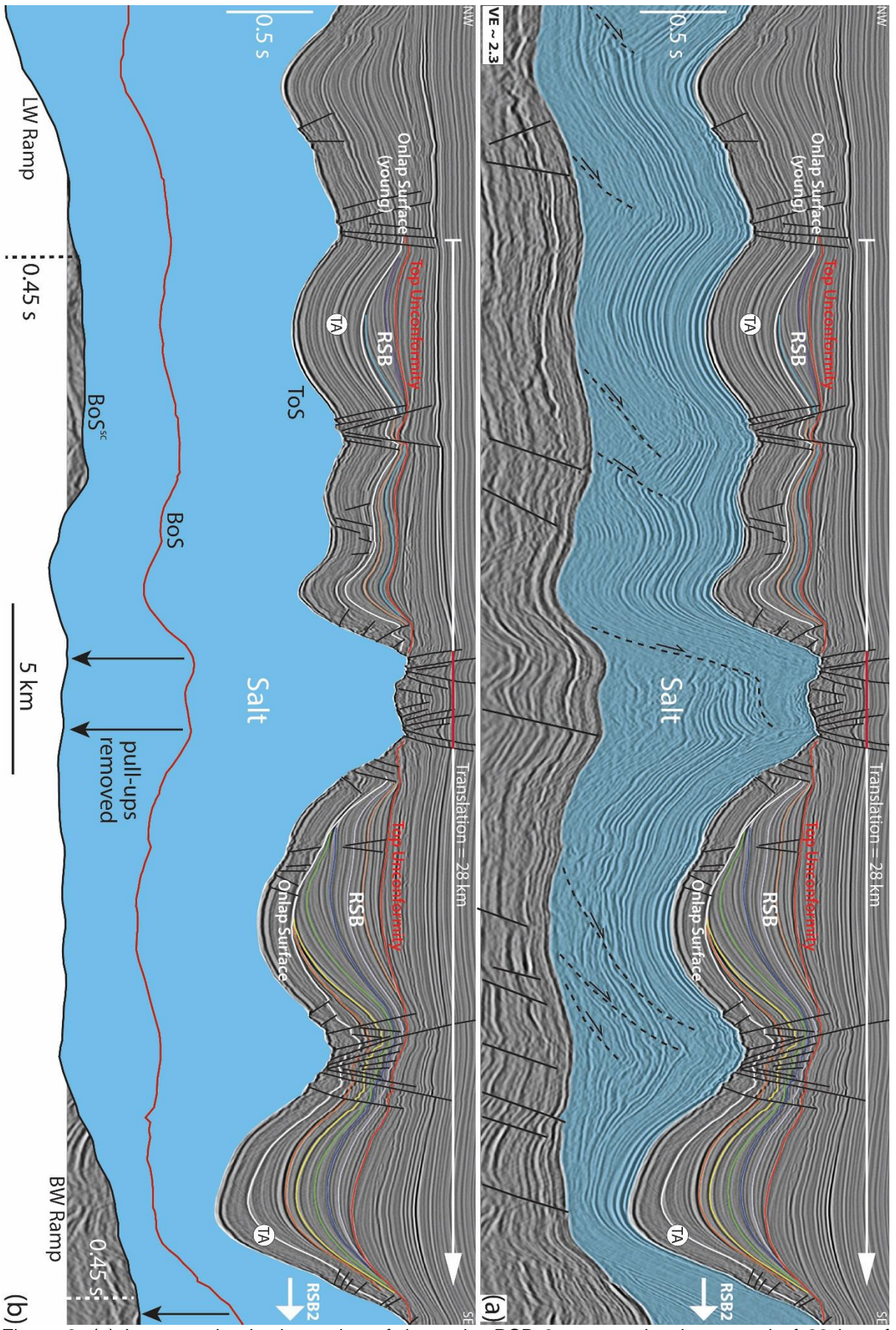
Figure 9: (a) Interpreted seismic section of the entire RSB 3 system showing a total of 28 km of

translation. In (b), RSB is displayed in combination with the static-corrected base-salt (BoS^{sc}) to demonstrate its relationship with base-salt topography and how this approach eliminates velocity artefacts due to high velocities of the salt interval. Base-salt structural relief is shown with TWT values in dashed-white lines below base-salt. The RSB is characterized by a well-defined and diachronous onlap surface (white) being onlapped by landward-dipping and thickening strata (colored lines) and truncated at the top by a diachronous unconformity (red). The basal onlap surface starts at the top Albian (TA) horizon and becomes progressively younger landward. RSB 3 is limited updip by a salt anticline formed above a landward-dipping base-salt ramp, and downdip by a large salt wall that also limits RSB 2 basinward. RSB 3 is segmented and folded by syn- to late diapirism. Faults are in black and pre-salt faults are used as a cross-check of base-salt structures. Base-salt structural relief is shown with TWT values in dashed-white lines below base-salt. Intra-salt shear zones (black dashed lines) indicate basinward movement and shear drag within the salt. For uninterpreted version, see supplementary material.
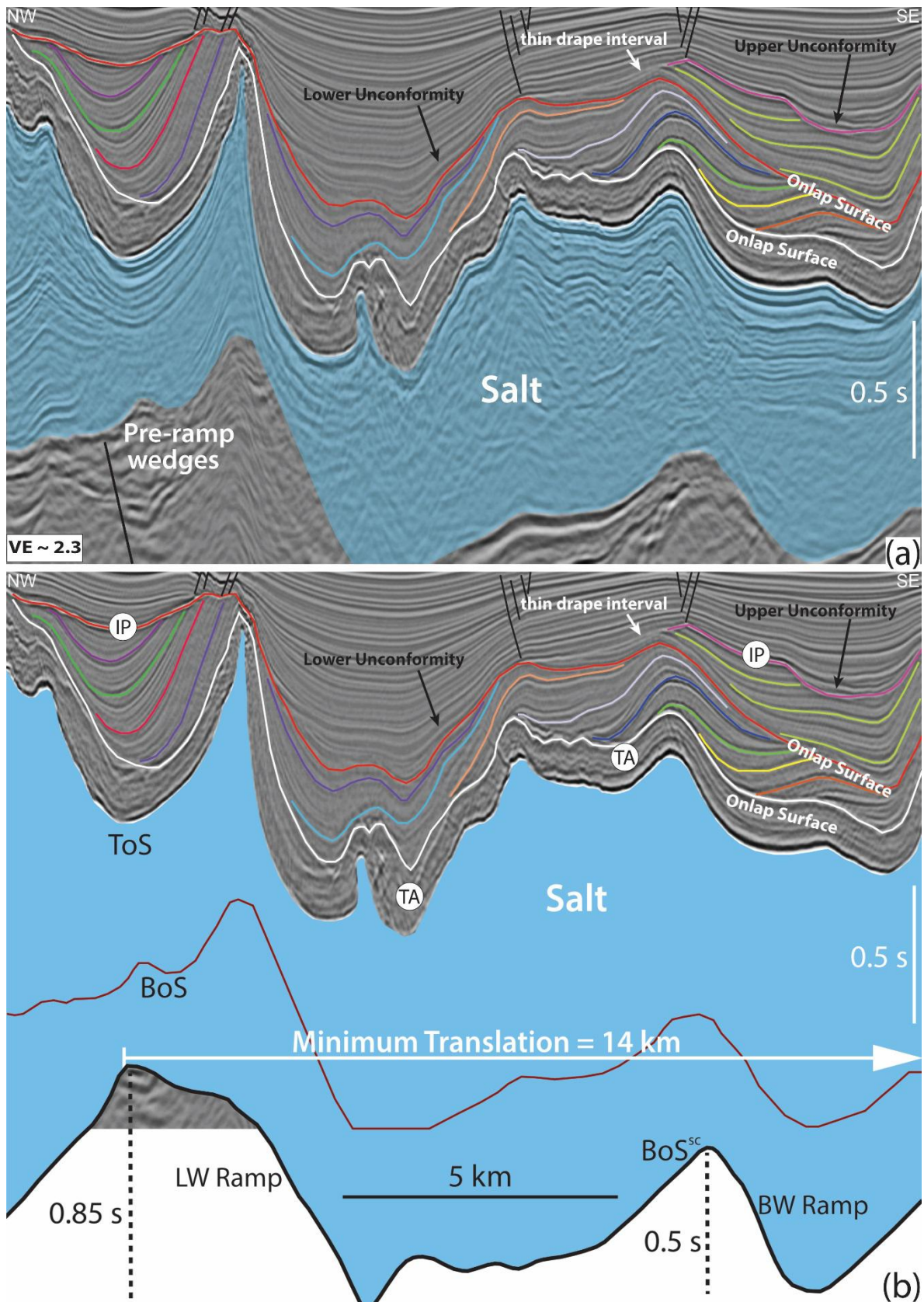
Figure 10: (a) Interpreted section of RSB 4 showing stacked RSBs and onlap surfaces (white and red). In (b) the stacked RSBs are show in the context of static-corrected base-salt (BoS^{sc}) and key horizons are presented: top Albian (TA), and intra-Paleocene unconformity (IP). Salt is in blue, faults in black and intra-RSB horizons in coloured lines. Onlap surfaces and top unconformity get slightly younger landward. Lower, landward RSB forms by translation over the landward-ramp (LW ramp) and

the upper, basinward RSB over the basinward-ramp (BW ramp). Top unconformity of lower RSB corresponds to the onlap surface of upper RSB (red) until becoming separated landward by a thin drape interval that is deposited updip of the basinward base-salt ramp and RSB. This surface (red) is aged mid-Cretaceous basinward and Intra-Paleocene landward evidencing its diachroneity. Base-salt structural relief is shown with TWT values in dashed- lines below base-salt. Only a minimum translation estimate of 14 km is obtained because RSB 5 is located at the edge of the data and is not visualized entirely. For uninterpreted version, see supplementary material.
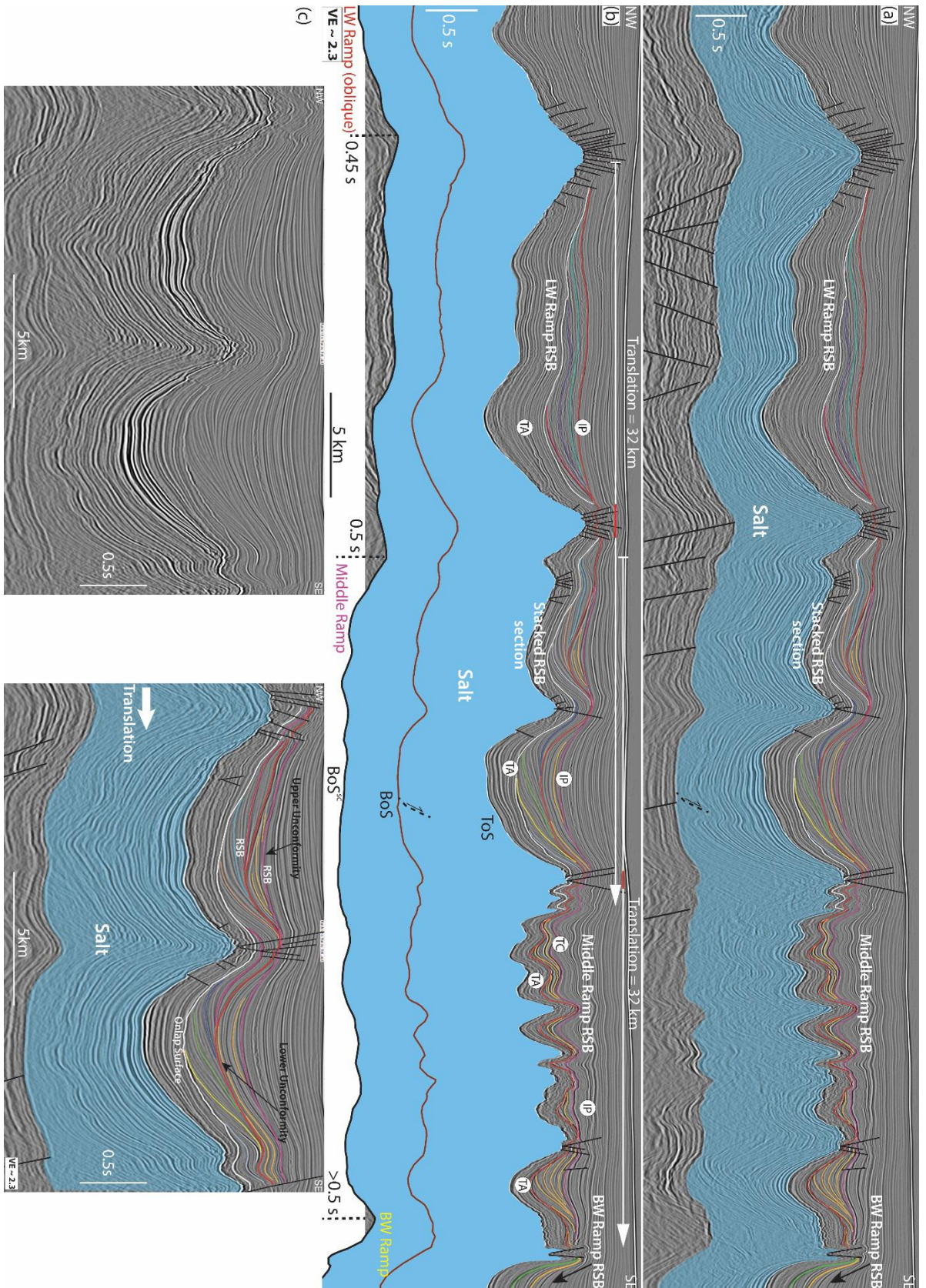
Figure 11: (a-b) Regional seismic sections of RSB 5 showing stacked RSBs and onlap surfaces (white and red lines) in the middle of the section. Salt is in blue and faults in black. In (b), the static-corrected base-salt (BoS^{sc}) and key horizons, top Albian (TA), top Cretaceous (TC) and intra-Paleoecene unconformity (IP) are presented. Three RSBs are shown: The basinwardmost one is

formed above a basinward-dipping ramp but appears only at the edge of the data. The middle RSB is formed by translation above a basinward-dipping ramp (middle ramp) and its landward portion is stacked on top of the basinward portion of the third, landward RSB, which is formed above a landward-dipping ramp. These RSBs are strongly affected by synchronous diapirism, folding and faulting but still show the typical geometries of RSB systems with sigmoidal landward-dipping and expanding strata. Base-salt structural relief is shown with TWT values in dashed-lines below base-salt. In (c), uninterpreted and interpreted localized sections of RSB 5, showing a zoom of the stacked RSBs section. A total of 32 km of translation is estimated for each of the stacked RSBs. The fact that both RSBs record the same amount of translation can be used as a cross-check for this measure. For complete uninterpreted version, see supplementary material.
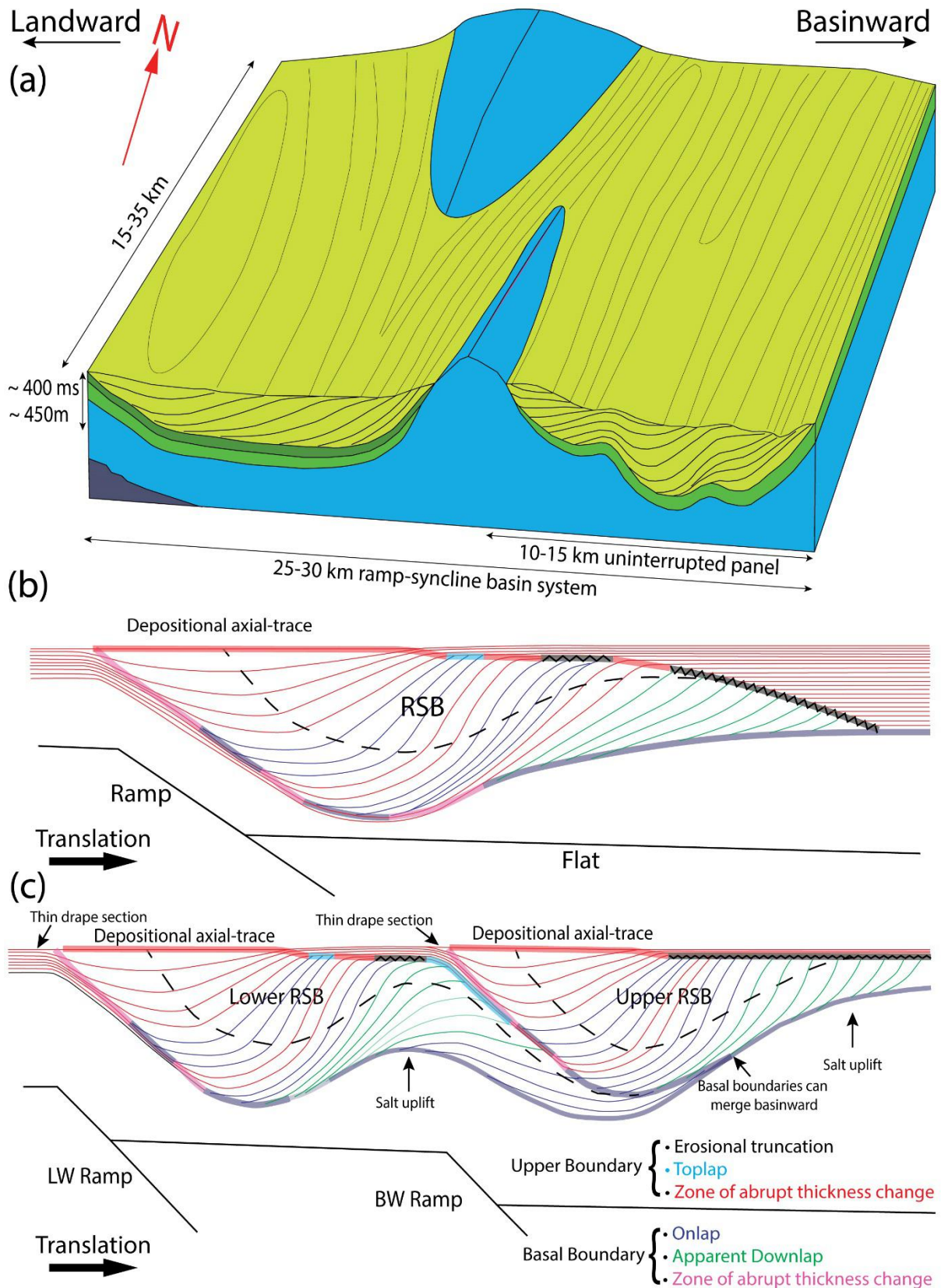
Figure 12: (a) Schematic 3D diagram of RSBs geometries, dimensions and relationship with diapirs and base-salt steps. (b) Summary of the 2D stratigraphic architecture showing the typical variations of strata termination of RSBs in the Santos Basin. The basal surface has terminations ranging from: i) abrupt apparent downlap at basinward edge, ii) abrupt onlap and iii) transition from thicker and

steeper section within the RSB to a thin draping interval at its landward edge. The top unconformity has a similar pattern of terminations ranging from abrupt erosional and toplap terminations downdip, to more transitional strata geometries updip. In (c), summary of the 2D stratigraphic architecture and strata terminations of stacked RSBs. The lower RSB finishes landward above the top of the landward ramp and the upper RSB finishes above the top of the basinward ramp. Stratal termination is similar to simple RSBs, but the lower RSB top unconformity acts as the onlap surface of the upper RSB along most of its length. A thin drape section can separate these surfaces at the upper RSB landward edge.
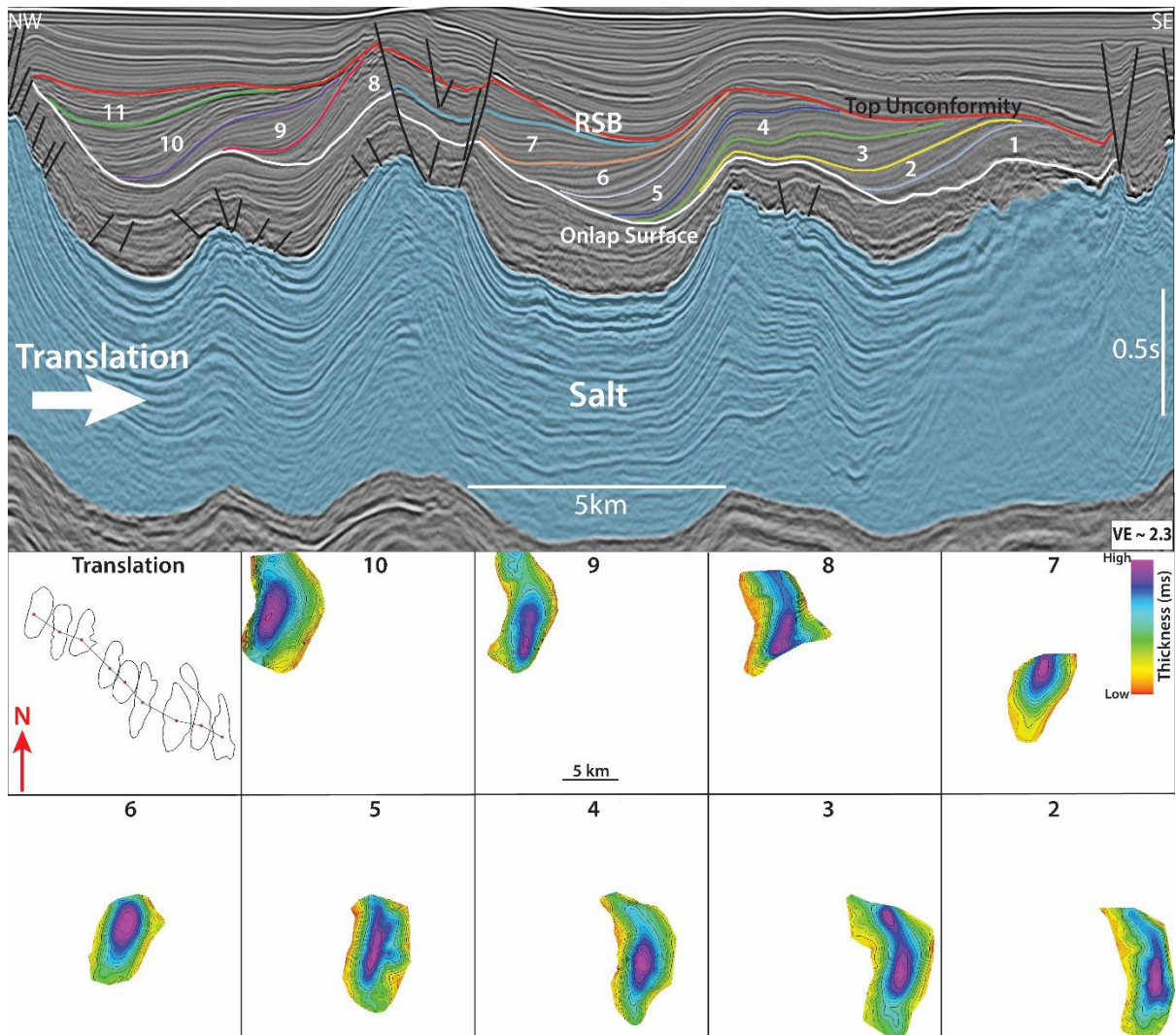
Figure 13: Interpreted seismic section of RSB 5 showing typical landward-dipping sigmoidal intervals and respective thickness maps illustrating the 3D kinematics of the system with 26.9 km of translation towards SE (120 $\pm$ 15 azimuth). Oldest intervals are located further downdip of the associated base-salt ramp. Thickness maps of intervals 1 and 11 are not shown because these intervals are affected by a higher degree of salt-related folding and faulting, which hinders the generation of confident maps.
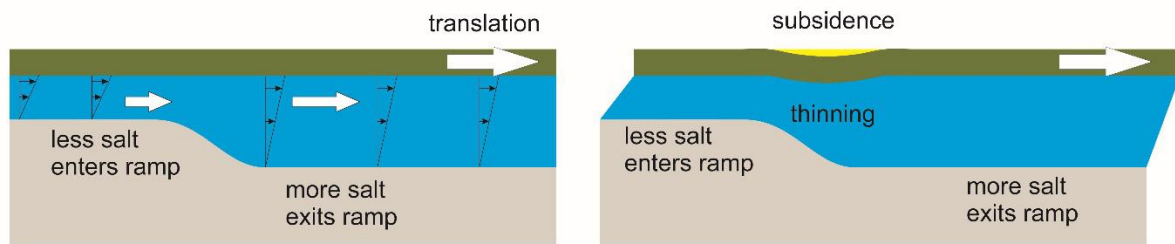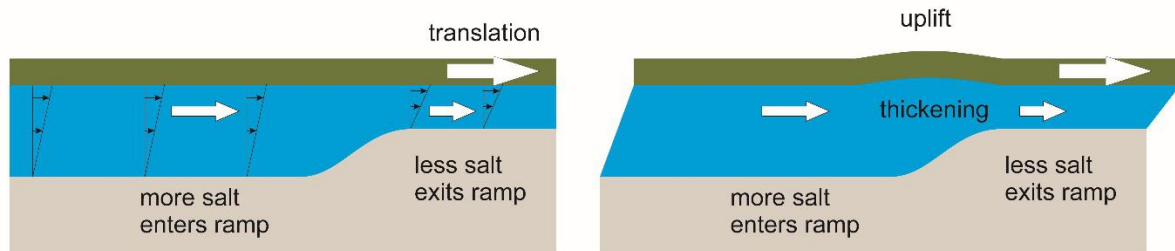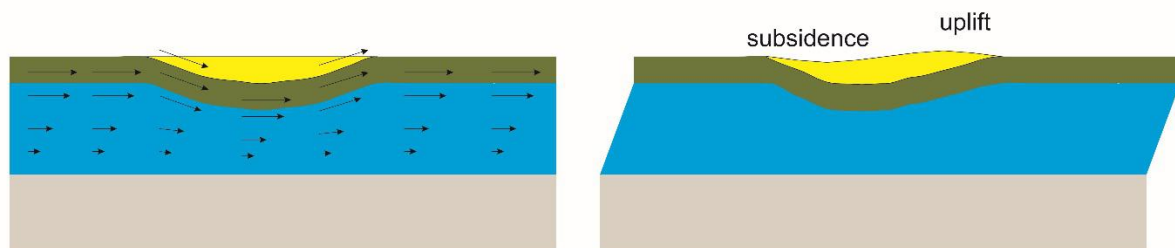
Figure 14: Conceptual 2D diagrams of the dynamics of Couette salt flow and variation of total salt-flux over a base-salt (a) basinward-dipping ramp and (b) landward-dipping ramp. In (a) the amount of salt leaving the ramp is lesser than the amount of salt arriving at the top of the ramp generating thinning of the salt layer, subsidence of the cover and generation of a depocentre immediately above the ramp. In (b), the amount of salt leaving the ramp is less than the amount of salt arriving, which results in salt thickening and uplift of the cover above the ramp. In (c), the diagram illustrates the effect of topography generated by translation above base-salt ramps by downward movement of the cover where the top-salt dips basinward and upward movement of the cover where the top-salt interval dips landward generating areas of local subsidence updip and uplift downdip.
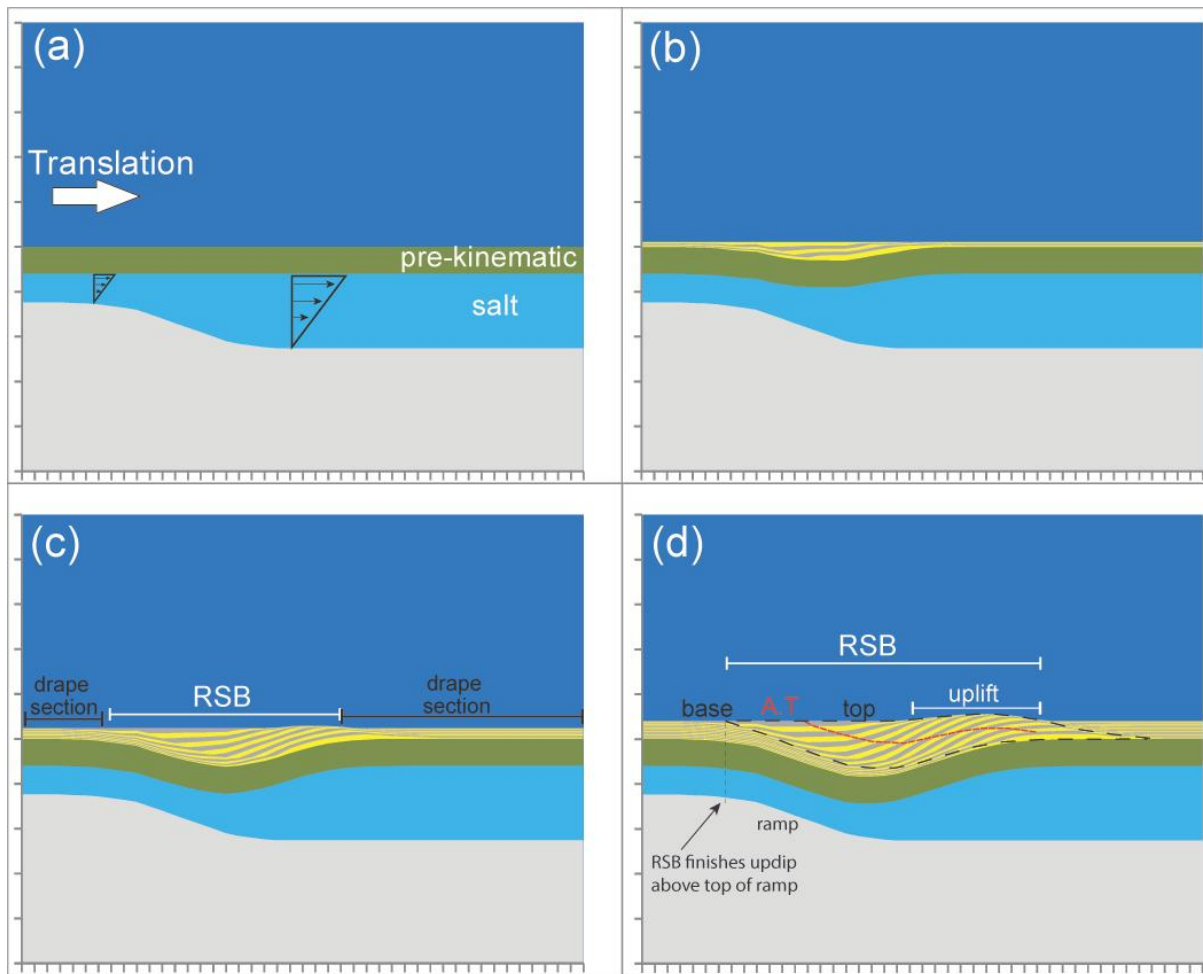
Figure 15: Numerical model simulating planar Couette flow and salt drag with overburden translation above a salt layer with a basal basinward-dipping ramp, which results in the development of a RSB above the ramp. Sequential evolution presented from (a) to (d). Syn-kinematic sediments are represented by yellow and grey layers.
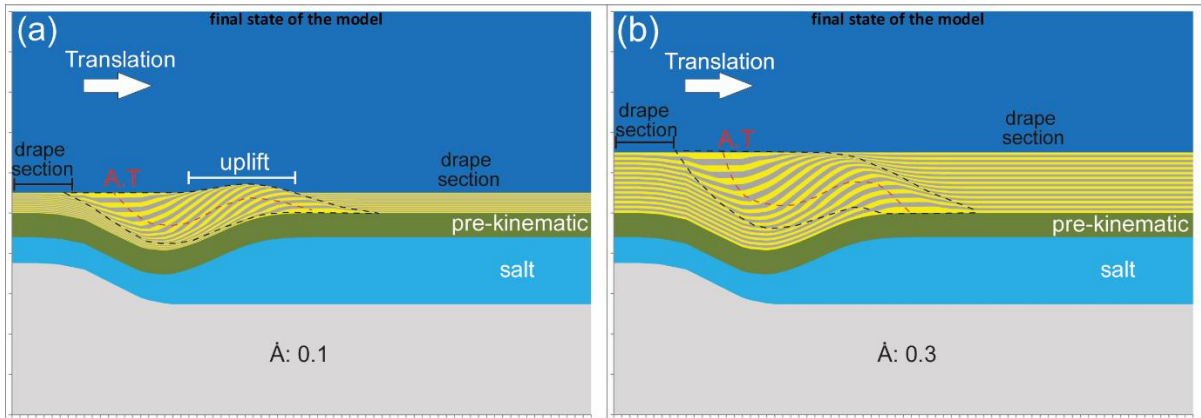
Figure 16: Final state of models simulating cover translation above a salt detachment with a base-salt ramp illustrating how variations of aggradation rate (□) can produce different stratigraphic architectures and stratal termination patterns. (□) in these models is non-dimensional so their variations are purely relative to translation rates (□). In (a) aggradation rate is 0.1 and the RSB is characterized by well-defined boundaries and uplift above the regional datum on the downdip side of the RSB. In (b) aggradation rate is 0.3 and the RSB is less asymmetric with upper and lower boundaries defined by a transition from thin section at regional dip to thicker and steeper section within the RSB. Translation rate (□) is the same in both models.
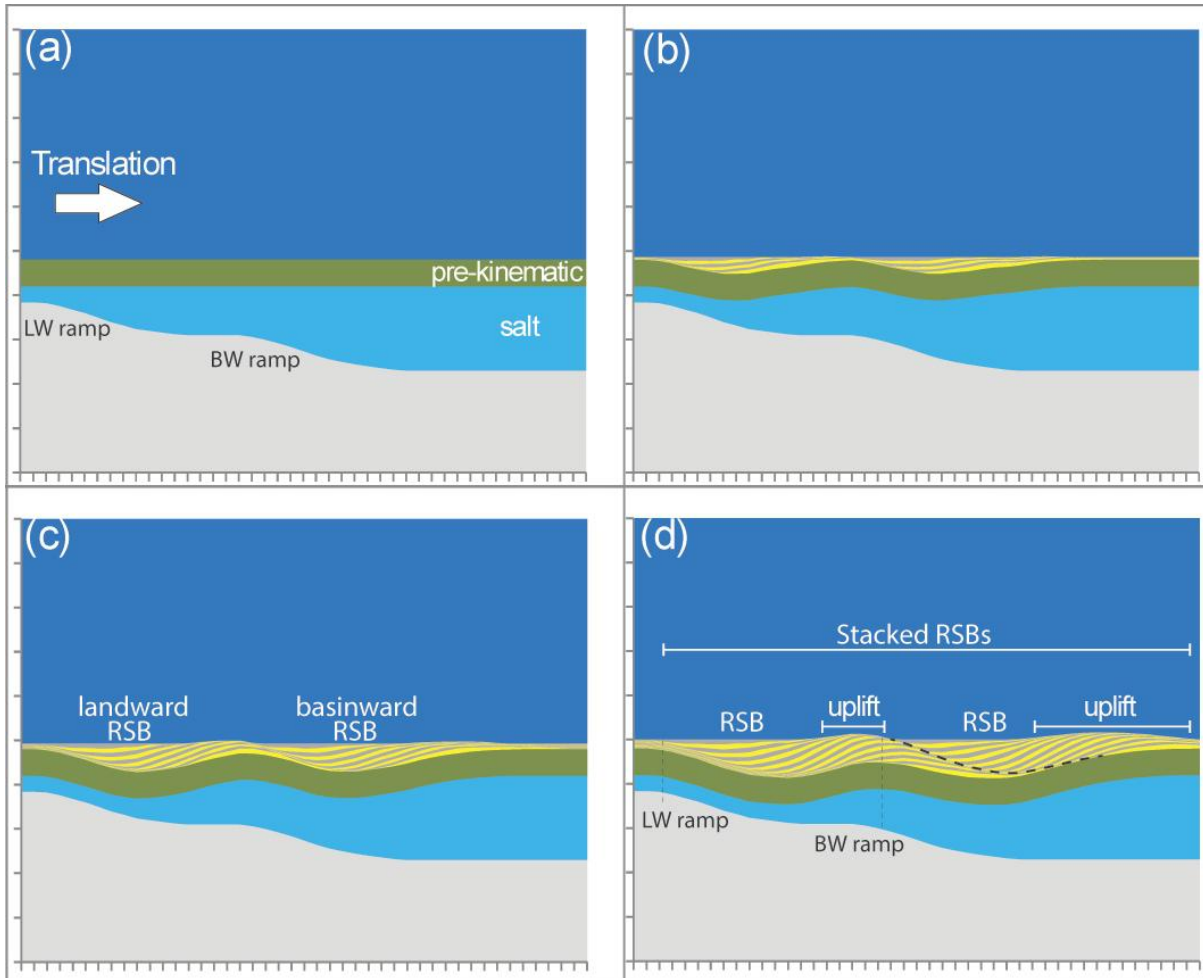
Figure 17: Numerical model simulating cover translation above a thick salt layer with 2 closely-spaced basinward-dipping ramps showing the sequential evolution of 2 stacked RSBs (a-d). The lower, landward RSB forms above the landward ramp while the upper, basinward RSB forms above the basinward ramp. Each of the RSBs finishes landward above their respective ramps. The top unconformity of the lower RSB acts as the onlap surface of the upper RSB (black dashed line). The upper and lower basal boundaries merge basinward while both top unconformities merge landward.
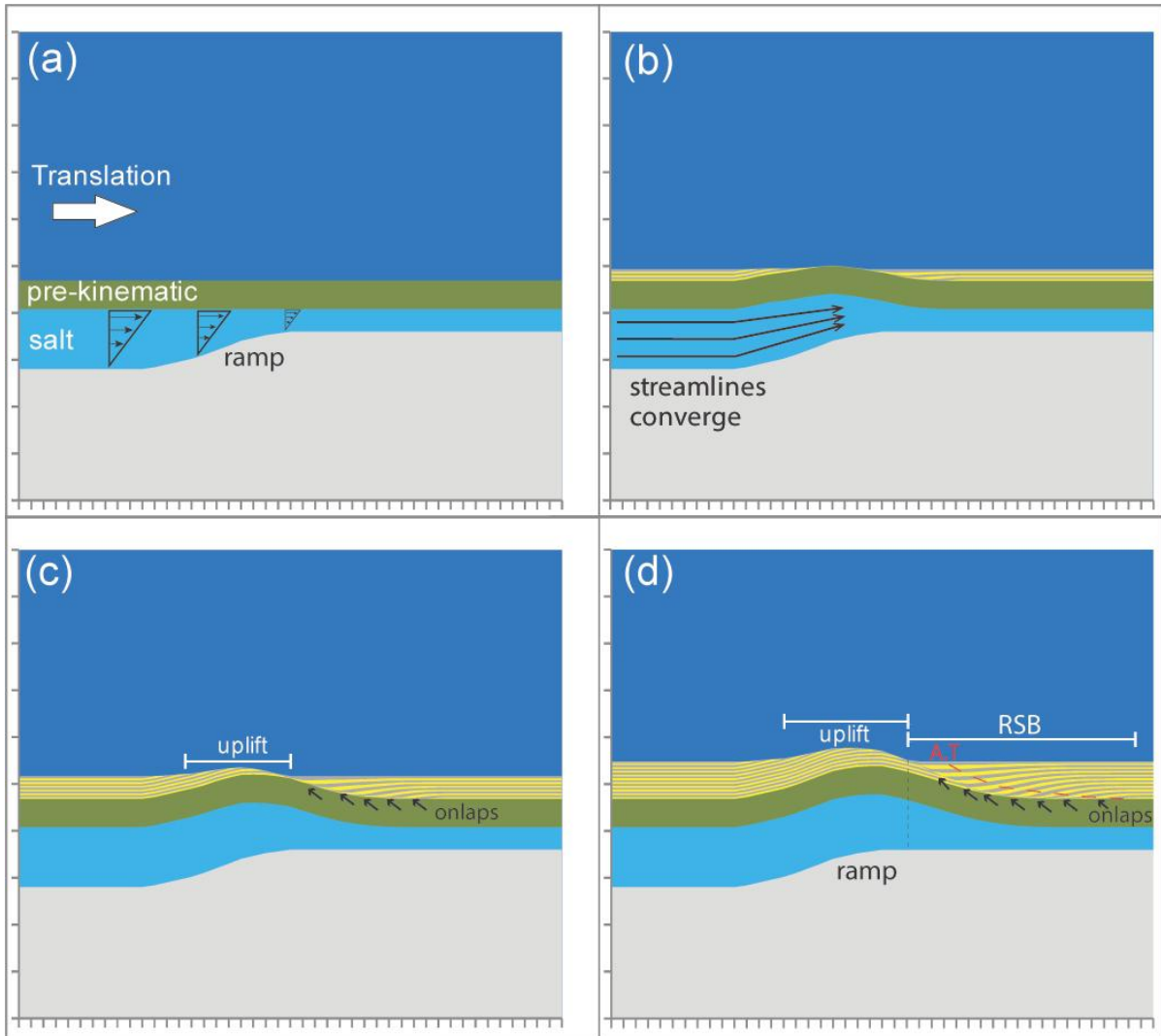
Figure 18: Numerical model simulating overburden translation and Couette salt flow above a landward-dipping base-salt ramp. Variations of salt flux across the step result in salt thickening over the ramp and development of a RSB basinward of it, above a base-salt flat. Sequential evolution is shown from (a) to (d).
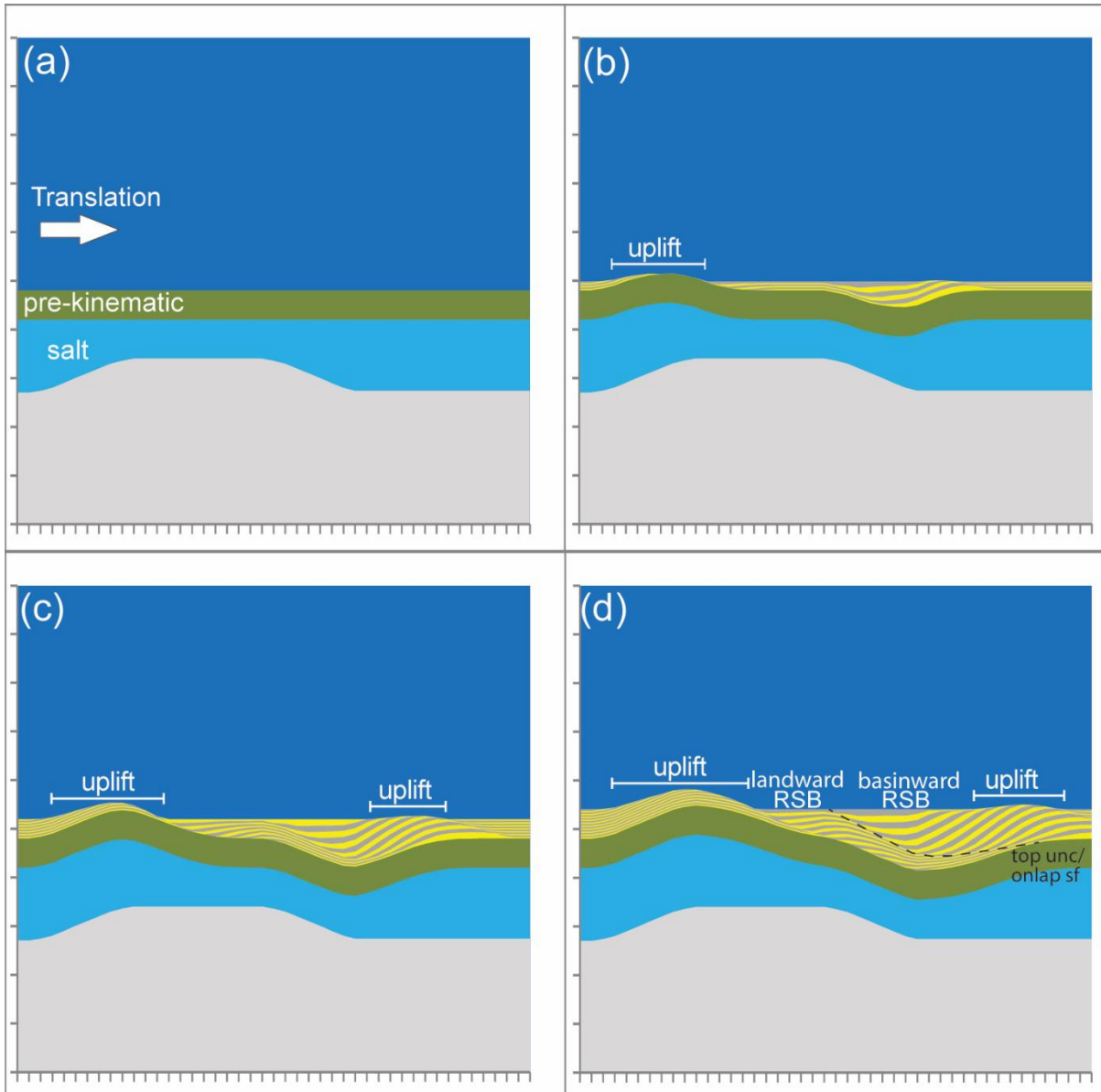
Figure 19: Numerical model showing the sequential evolution (a) to (d) of overburden translation and Couette-type salt flow above two oppositely dipping base-salt ramps and the development of hybrid stacked RSBs.

(a) Restored and decompacted to stratigraphic horizon "x", v=5h

SW

NE

Pre-RSB strata

Pre-salt sediments

Salt

Atlantic Hinge Zone

Basement?

(b) Present day depth structure, v=5h

RSB

Top

Base
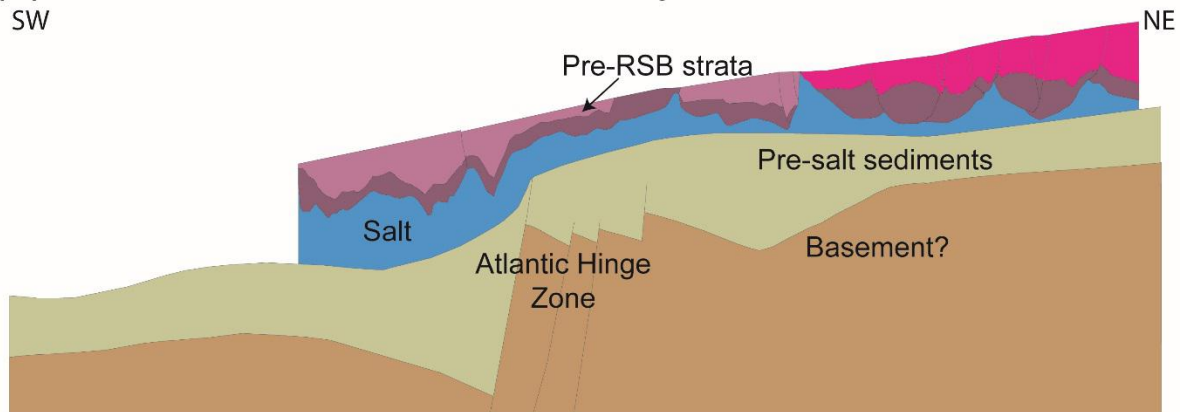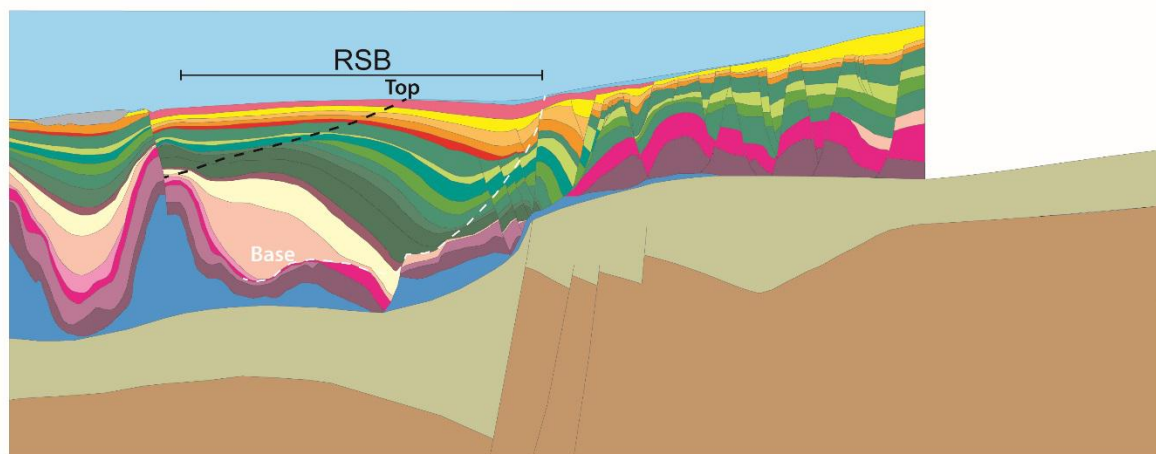
(c) Present day depth structure, v=h

| 0 | 10 | 20 | 30 | 40 | 50 | 60 | 70 | 80 km |
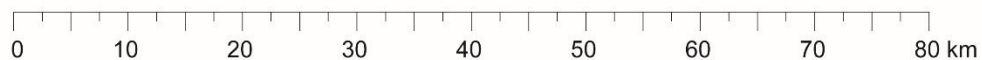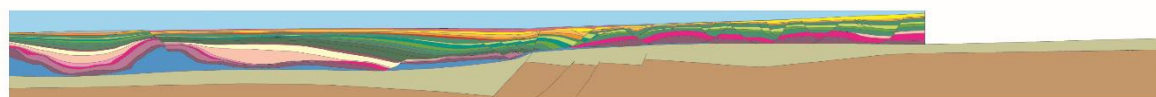
Figure 20: restoration of Line 214 from the Lower Kwanza Basin (adapted from Peel, 2014). Salt is in blue and RSB intervals are represented by colours ranging from purple, green, orange and yellow. RSB forms by translation over the Atlantic Hinge zone, which corresponds to a major basinward-dipping base-salt step. Original salt thickness varies from 1 km above the ramp to 2 km downdip. Translation is ongoing as the system is capped landward by the sea-floor. A total of 24 km of translation has been measured in this section.
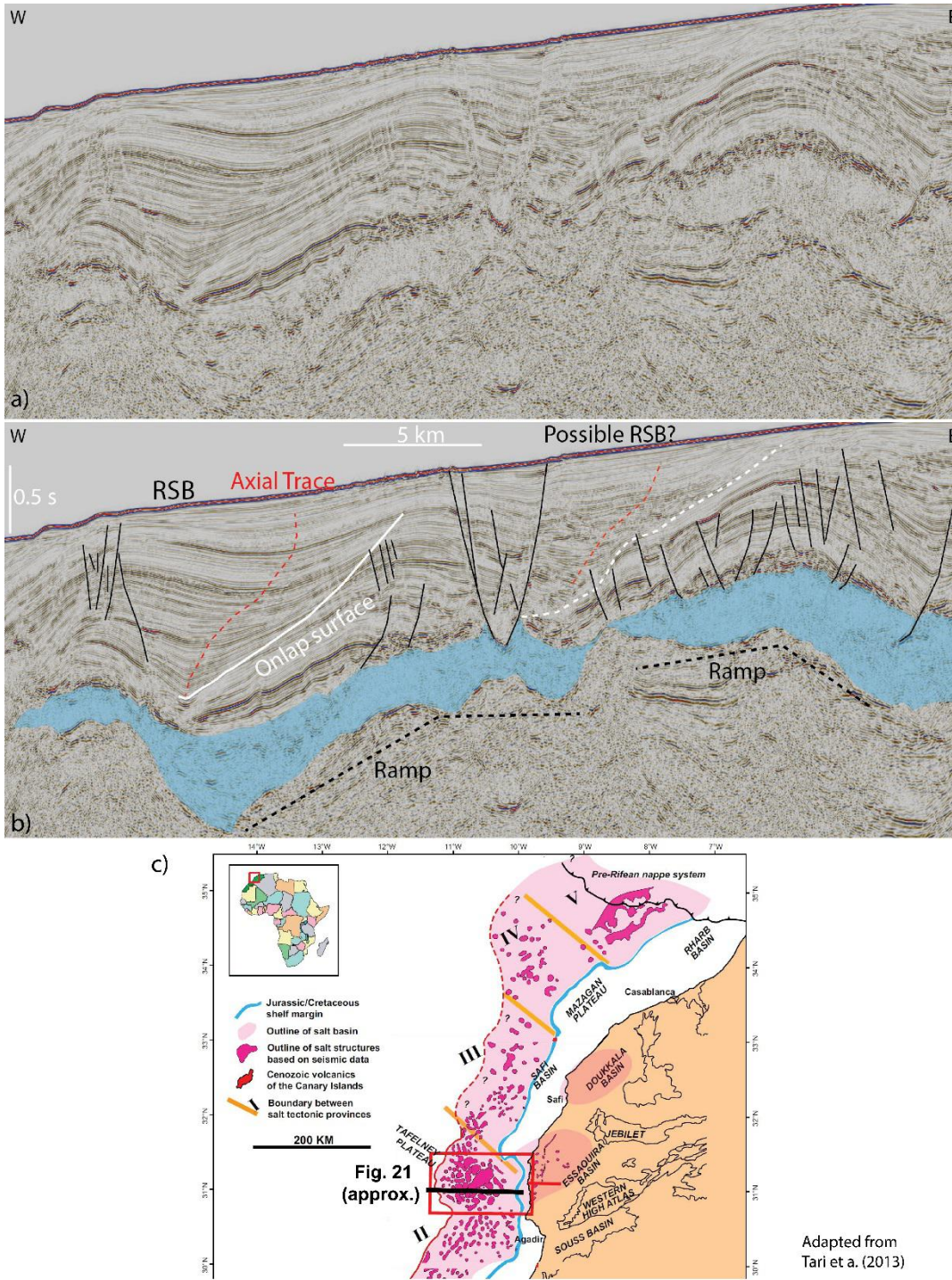
Figure 21: Uninterpreted (a) and interpreted (b) seismic sections showing a simple RSB formed above allochthonous salt (blue) with a base-salt basinward-dipping ramp in the Essaouira-Agadir Basin, Morocco. Another possible candidate of RSB appears to the East but the limited seismic resolution in the area hinders its clear identification. Approximate line location (black line) shown in map adapted from Tari et al. (2013) in (c).